Helvetica Physica Acta
Vol. 64 (1991)

0018-0238/91/050700-36$1.50+0.20/0

Monte Carlo Simulation of the One-Dimensional t-J-J' Model

Matthias Troyer

Interdisziplinäres Projektzentrum für Supercomputing
and Institut für theoretische Physik
ETH Zürich, Switzerland

(19. IV. 1991)

Abstract

I present a new and efficient disconnected cluster decomposition to perform Monte Carlo Simulations based on the Trotter-Suzuki method for 1-d quantum systems. As opposed to the normal checkerboard world line algorithm this mapping allows one to simulate models with interactions up to next nearest neighbours or even one-dimensional double layers. I have used this cluster decomposition to simulate the one-dimensional t–J–J' model at $\alpha = J'/J = 0.5$ and have investigated the sign problem in this model. At half band filling the system is dimerised into singlet spin pairs when $\alpha = 0.5$ due to frustration. I believe that the spin gap is no longer present around quarter band filling. Instead the system shows a $2k_f$ spin density wave and a $4k_f$ charge density wave for low values of J/t. At higher values of J/t the system is phase separated but there is a region where there are still holes in the particle rich phase. At large values of J/t the system will be separated into a dimerised Heisenberg chain and a sea of holes.

Table of Contents

I Introduction

The discovery of high-T_c superconductors by Bednorz and Müller [1] has probably been the most surprising event in solid state physics in the last decade. The mechanism producing superconductivity in these system is not yet understood. All these newly discovered superconductors have one structure element in common. There are two-dimensional planes of CuO_2. They consist of four-fold coordinated Cu ions surrounded by four two-fold coordinated O ions. In undoped materials there is one hole on each of the Cu sites. Doping introduces extra holes that reside primarily on the O sites. However hybridisation binds the hole strongly to the central Cu^{2+} ion, forming a local singlet together with the hole already on the Cu ion [2]. An important questions is which microscopic Hamiltonian correctly describes the various states of these materials.

Anderson [3] proposed a Hamiltonian with strong on-site Coulomb interactions among the electrons in the partially filled band of Cu $3d$ levels. A simplification of this Hamiltonian leads to the single band Hubbard model. The one-dimensional Hubbard model was solved exactly some time ago [4,5]. Some simulations have been done on small two-dimensional systems. In the limit $U/t \to \infty$ the Hubbard model becomes the low J/t limit of the $t-J$ model [6]. Zhang and Rice [2] have also derived the $t-J$ model as an effective Hamiltonian of a two band Hubbard model. But the $t-J$ model is interesting not only in the limit $J \to 0$ where it is the large U limit of the Hubbard model but at other values of J/t as well.

At $J/t = 0$ the one-dimensional $t-J$ model can be solved exactly since in that case it is the large U limit of the Hubbard model. At $J/t = 2$ the $t-J$ model can also be solved exactly by a Bethe Ansatz [7]. At other values of J/t one has to use numerical methods [8,9].

Although the copper oxide planes are two-dimensional systems much work has been done on one-dimensional systems. They are easier to calculate than two-dimensional systems and show a very rich phase diagram [8,9]. It is expected that two-dimensional systems should share some properties of the one-dimensional systems. As it is difficult to simulate two-dimensional systems an intermediary step can be taken and a next nearest neighbour interaction added to a one-dimensional system. This introduces some effects of two-dimensional

systems, e.g. a next nearest neighbour antiferromagnetic interaction frustrates a Heisenberg antiferromagnet. Frustration is a typical phenomena in higher dimensional systems.

Many of the models investigated are single band models. There one uses a lattice with one site per Cu ion. This lattice is partially filled with spin-$\frac{1}{2}$ fermions (the holes in the Cu $3d$ band). In the undoped case this band is half filled (on average one particle per site). Doping reduces the number of particles since, as mentioned above, some of the holes in the Cu $3d$ band form local singlets with holes introduced by doping. I have considered the one-dimensional $t-J-J'$-model on a chain of length L, where L is a multiple of four:

$$\begin{aligned} H &= -t\sum_{i=1}^{L}\sum_{\sigma=\pm 1/2} h^{\dagger}_{i+1,\sigma}h_{i,\sigma} + h.c. \\ &\quad + J\sum_{i=1}^{L}(\vec{S}_i\vec{S}_{i+1} - \frac{1}{4}n_in_{i+1}) + \alpha J\sum_{i=1}^{L}(\vec{S}_i\vec{S}_{i+2} - \frac{1}{4}n_in_{i+2}). \end{aligned} \tag{1}$$

Here $L+1 \equiv 1, L+2 \equiv 2$, $\vec{S}_i$ is the spin operator and n_i the particle number operator at the site i. $h^{\dagger}_{i,\sigma}$ is the pseudo fermion creation operator

$$h^{\dagger}_{i,\sigma} = (1-n_{i,-\sigma})c^{\dagger}_{i,\sigma},$$

where $n_{i,-\sigma}$ is the number of particles at the site i with z-component of spin $-\sigma$. $c^{\dagger}_{i,\sigma}$ creates a particle on site i with z-component of spin σ. Due to the projector in $h_{i,\sigma}$ double occupancy is prohibited. The particles on the lattice are allowed to hop between adjacent sites. They are submitted to a nearest neighbour Heisenberg interaction with strength J and a next nearest neighbour Heisenberg interaction with strength $J' = \alpha J$. In the limit $\alpha = 0$ the model reduces to the $t-J$ model and at half band filling to a Heisenberg linear chain with next nearest neighbour interaction.

Many of the interesting strongly correlated quantum mechanical systems cannot be solved exactly. As they contain strong interactions perturbation theory cannot be used either. Therefore numerical methods have to be used. It is well known since more than twenty years how classical systems can be simulated. Most of the methods used are based on the Metropolis algorithm [10]. Simulating quantum mechanical systems is a more difficult task. One problem is that the Metropolis algorithm requires the calculation of the weight of a configuration. In a classical system the weight of a configuration in the canonical ensemble is simply given by $e^{-\beta E}$, where β is the inverse temperature and E is the energy of the

configuration. In a quantum mechanical system however the weight of a state $|\Psi\rangle$ is given by $\langle\Psi|e^{-\beta H}|\Psi\rangle$, where H is the Hamiltonian of the system. Direct evaluation of this weight requires a diagonalisation of the system. And this is exactly what one wants to avoid by using the Monte Carlo method. One way to calculate properties of quantum mechanical systems is of course exact diagonalisation (e.g. by Lanczos algorithm [9]). By this method the energy of the ground state and of the first few excited states can be calculated exactly. The method is restricted to systems with a small number of states and there is no direct method to calculate the spin and charge structures from these energies. To calculate the spin and charge structure factors one has to be able to make further assumption, e.g. that the model scales to a Tomonaga-Luttinger liquid. Only then the critical exponents and the spin and charge structure factors can be calculated.

Other methods are based on the Trotter-Suzuki theorem [11,12]. Using the Trotter formula one can map the d-dimensional quantum mechanical system onto a $d+1$-dimensional classical system. Then a transfer matrix method or the world line algorithm [13] can be used to simulate the system. A disadvantage of the method which can be seen immediately is that the dimension of the system has increased. To get information on a one (two)-dimensional quantum mechanical system one has to simulate a two (three)-dimensional classical one. This method can be used for much larger systems and the correlations and structure factors can be calculated directly. However as the algorithm works at finite temperatures it is necessary to extrapolate to $\beta \to \infty$ to get the ground state properties. There can be numerical difficulties due to a sign problem if there are fermionic degrees of freedom. This problem is serious at low temperatures and for large lattices. A combination of both methods can be very helpful. This was done in investigations of the $t-J$ model [8,9]. The decompositions of the Hamiltonian that have previously been used with the transfer matrix method or the world line algorithm are restricted to nearest neighbour interactions. In order to simulate the $t-J-J'$ model or other models with next nearest neighbour interactions a new decomposition of the Hamiltonian has to be found and the algorithms have to be adapted. The algorithm developed can then be used to simulate one-dimensional systems with arbitrary next nearest neighbour interactions. There are also some advantages when simulating models with nearest neighbour interactions only.

II Path Integral Formulation and World Lines

The world line algorithm I have used to simulate the system relies on a decomposition of the Hamiltonian into two sums H_1 and H_2, each of which consists of a sum of commuting terms. I used the relation

$$e^{\epsilon(A+B)} = e^{\epsilon(A/2+B+A/2)} = e^{\epsilon A/2} e^{\epsilon B} e^{\epsilon A/2} + \mathrm{O}(\epsilon^3)$$

and Suzuki's generalisation of the Trotter formula [11,12] to calculate the partition function:

$$\begin{aligned} Z &= \mathrm{Tr}\left(e^{-\beta H}\right) = \mathrm{Tr}\left((e^{-\Delta\tau(H_1+H_2)})^M\right) = \\ &\mathrm{Tr}\left((e^{-(\Delta\tau/2)H_1} e^{-\Delta\tau H_2} e^{-(\Delta\tau/2)H_1} + \mathrm{O}(\Delta\tau^3))^M\right) = \\ &\mathrm{Tr}\left((e^{-\Delta\tau H_1} e^{-\Delta\tau H_2})^M\right) + \mathrm{O}(\Delta\tau^2) = \\ &\sum_{i_1,\ldots,i_{2M}} \langle i_1|U_1|i_{2M}\rangle\langle i_{2M}|U_2|i_{2M-1}\rangle \cdots \langle i_3|U_1|i_2\rangle\langle i_2|U_2|i_1\rangle + \mathrm{O}(\Delta\tau^2), \end{aligned} \tag{2}$$

where β is the inverse temperature (imaginary time) and $\Delta\tau = \beta/M$. The $|i_k\rangle$ are a complete orthonormal system of the states in real space,

$$U_1 = e^{-\Delta\tau H_1} \quad \text{and} \quad U_2 = e^{-\Delta\tau H_2}.$$

The decomposition thus leads to a systematic error of order $(\Delta\tau)^2$. The state $|i_1\rangle$ evolves in imaginary time (inverse temperature, called Trotter direction) according to the time evolution operators U_1 and U_2. Since H_1 and H_2 are sums of commuting terms the time evolution operator breaks up into a product of small cluster operators. The evaluation of the matrix elements $\langle i|U_1|i'\rangle$ reduces to solving this finite cluster problem.

A The Cluster Decomposition

The simplest decomposition of the Hamiltonian is the checkerboard decomposition (disconnected bonds). There the Hamiltonian is split into two sums, each consisting of two-particle terms (figure 1a). However this decomposition cannot be used for models with next nearest neighbour interactions. Here I present a decomposition for one-dimensional quantum chains with hopping and spin interactions between nearest neighbours and next nearest neighbours.

a) Checkerboard decomposition

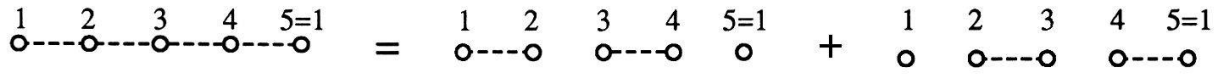

b) Decomposition for a model with next neighbour interactions:

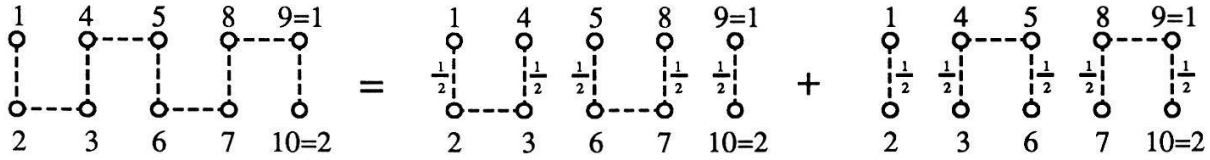

c) Decomposition for a model with next neighbour and next nearest neighbour interactions:

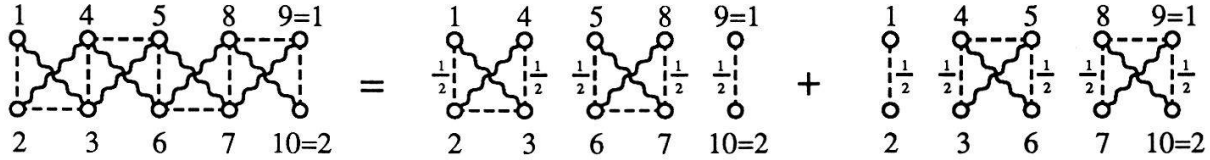

d) Decomposition for a double layer:

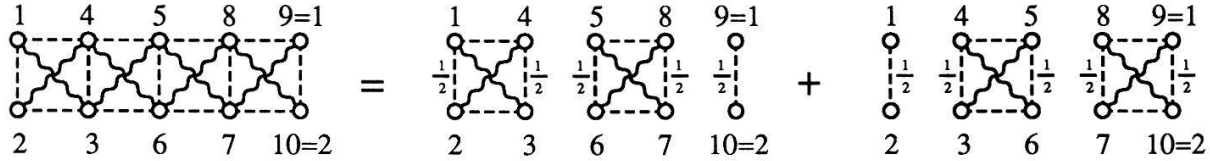

Figure 1. Decomposition of the Hamiltonian. Next neighbour interactions are denoted by dashed lines,next nearest neighbour interactions by wiggled lines. The $\frac{1}{2}$ besides an interaction indicates, that only half of the interaction is contained in this term.

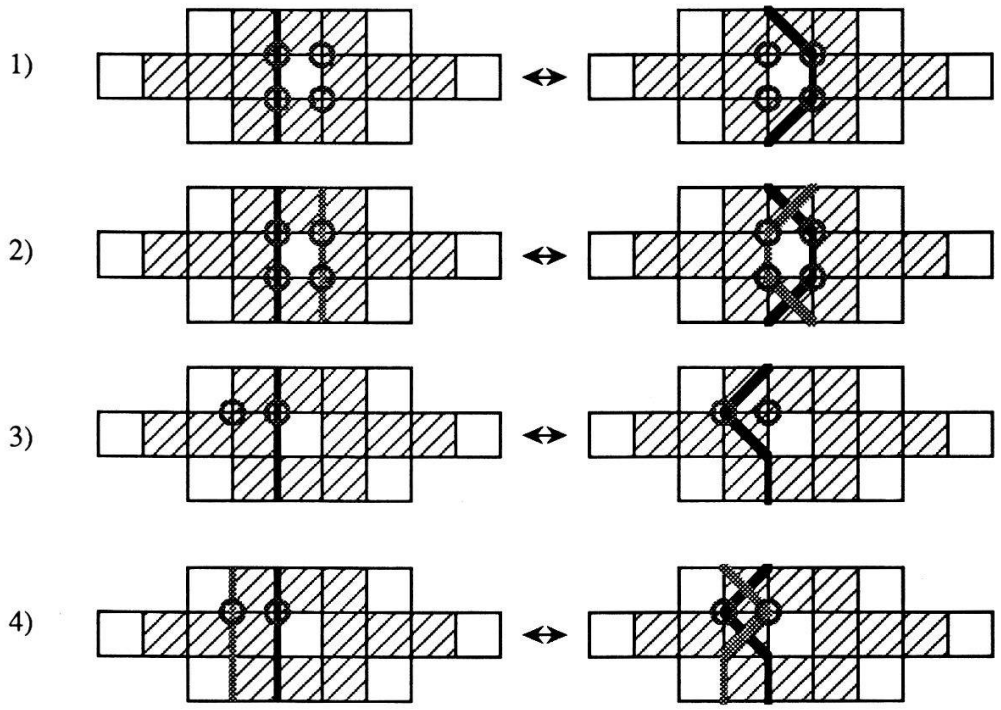

Figure 2. Examples of the moves used to upgrade a world line configuration. Circles denote the sites that are affected by the move. See text for details.

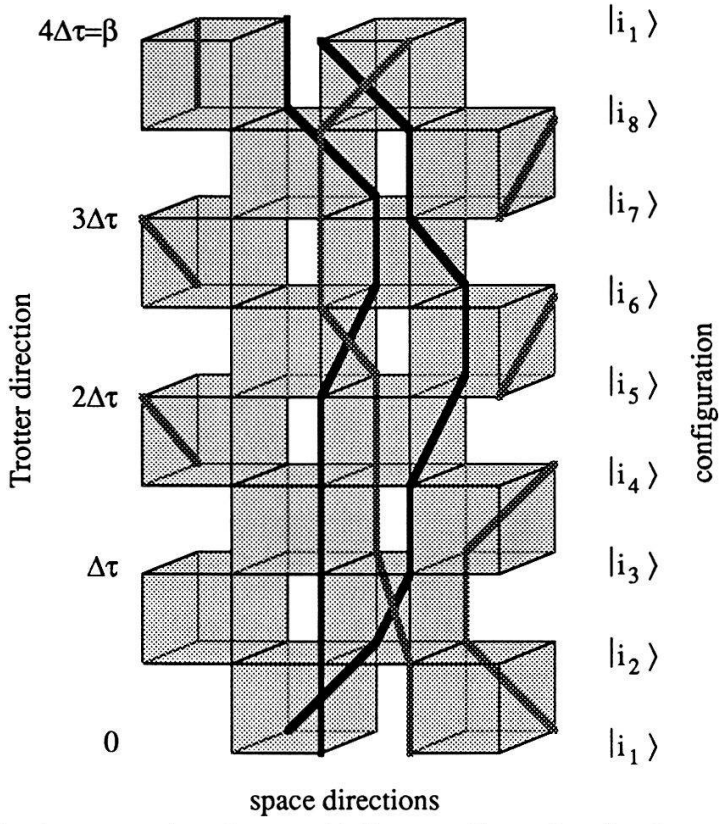

Figure 3b. An example of a world line configuration in three dimensional representation. The imaginary time (Trotter direction) runs along the vertical axis.

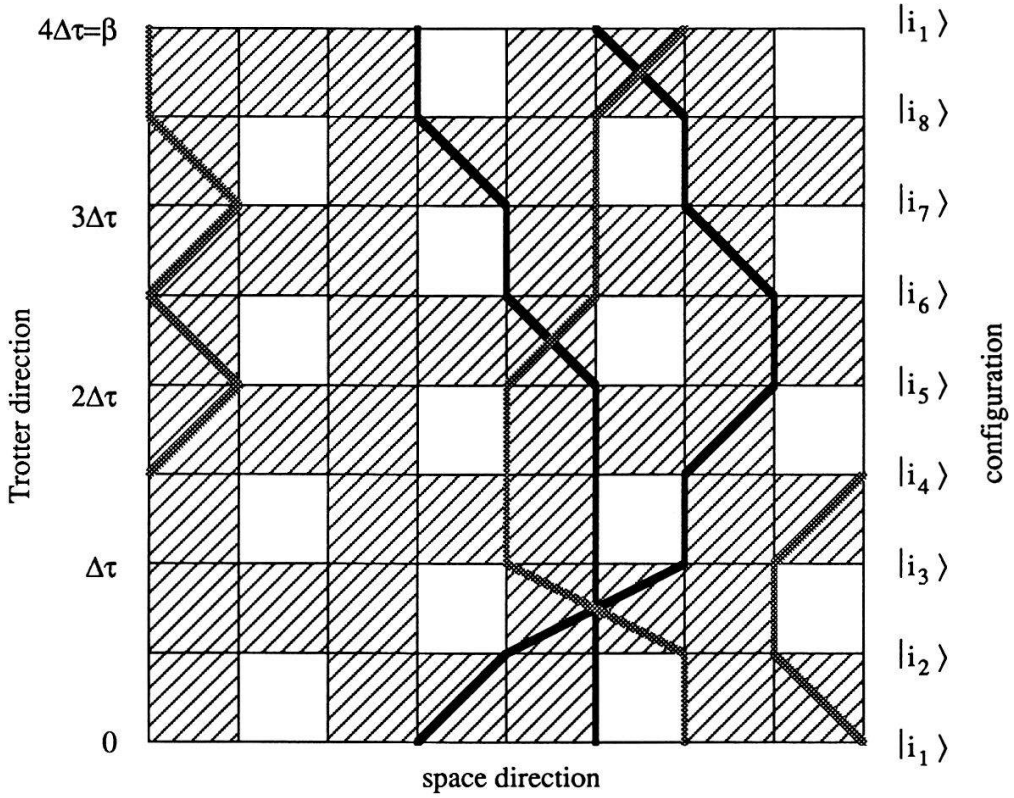

Figure 3b. An example of a world line configuration in two dimensional representation. The imaginary time (Trotter direction) runs along the vertical axis.

Models that can be simulated with this algorithm include the Heisenberg model, free electrons, the $t-J$ model, the $t-J-J'$ model, the $t-t'-J$ model, etc.. The decomposition of the Hamiltonian is best shown by arranging the sites on a double layer (see figure 1 b,c). The Hamiltonian is split into two sums of 4-particle terms. The interactions in the odd numbered squares are collected in one term and the interactions of the even numbered terms in the second term. One sees immediately that the same algorithm can be used to simulate a double layer (figure 1d).

In the case of the $t-J-J'$ model the Hamiltonian (1) is split into the two sums:

$$H_1 = \sum_{\substack{1\le i\le L/2 \\ i \text{ even}}} H_{(i)}, \qquad H_2 = \sum_{\substack{1\le i\le L/2 \\ i \text{ odd}}} H_{(i)},$$

where

$$\begin{aligned} H_{(i)} = & -t\sum_{\sigma}(\frac{1}{2}h^{\dagger}_{2i-1}h_{2i} + h^{\dagger}_{2i}h_{2i+1} + \frac{1}{2}h^{\dagger}_{2i+1}h_{2i+2} + h.c.) \\ & +\frac{J}{2}(\vec{S}_{2i-1}\vec{S}_{2i} - \frac{1}{4}n_{2i-1}n_{2i}) + J(\vec{S}_{2i}\vec{S}_{2i+1} - \frac{1}{4}n_{2i}n_{2i+1}) \\ & +\frac{J}{2}(\vec{S}_{2i+1}\vec{S}_{2i+2} - \frac{1}{4}n_{2i+1}n_{2i+2}) \\ & +\alpha J(\vec{S}_{2i-1}\vec{S}_{2i+1} - \frac{1}{4}n_{2i-1}n_{2i+1}) + \alpha J(\vec{S}_{2i}\vec{S}_{2i+2}) - \frac{1}{4}n_{2i}n_{2i+2}). \end{aligned} \tag{3}$$

The evaluation of the weight of a configuration is thus reduced to solving a 4-particle system in the subspaces of constant spin and particle number. This was done numerically (see Appendix).

Within each time interval $\Delta\tau$ there is one application of the evolution operator U_1 and one of the evolution operator U_2. This leads to a graphical representation of the above sum (2) on a two-dimensional double layer, where the applications of the time evolution operator on a square are marked by shaded cubes (figure 3a). The occupation on each time slice corresponds to one of the states $|i_k\rangle$ in the sum for Z. As the time evolution operator conserves particle number and total magnetisation we can connect the occupied sites on neighbouring Trotter slices and get a representation of the configuration $\{|i_k\rangle\}$ in terms of world lines. The sum over all configurations $\{|i_k\rangle\}$ with non zero weight thus corresponds to the sum over all possible world line configurations. There are two kinds of world lines

(black and gray) representing up and down spins that follow the imaginary time evolution of the spins as shown in figure 3. The time evolution operators act independently on every elementary square. Hopping or spin flips can occur only within shaded cubes but not within unshaded ones. The configurations can as well be drawn on a two-dimensional lattice by arranging the sites on a straight line and not in a double layer (figure 3b).

The Metropolis algorithm may then be used to upgrade a world line configuration. The only possible moves to upgrade the configuration are those that do not break world lines as otherwise the weight of the new configuration is zero. I have employed four types of moves (see figure 2): 1) moves around an unshaded square, where one world line is moved from one side of the square to the other or 2) two world lines of opposite spin are interchanged; 3) moves along a bond to the left or right of an unshaded square, where the particle is shifted along that bond or 4) two particles with opposite spin are interchanged. The moves that are shown in figure 2 are examples of these moves. The sites that are affected by the move are marked with a gray circle. The occupation of the other site is arbitrary. It has influence on the weight of the configuration but not on the move itself. The move just exchanges particles on the affected sites. After the exchange new world lines can be drawn in any case as the particle number and magnetisation are conserved within each of the cubes.

These moves conserve the total particle number and magnetisation as well as the winding number of the world lines. When one knows that the ground state is a spin singlet the z-component of the total spin can be chosen to be zero. If the spin of the ground state is nonzero or if one wants to do calculations at higher temperatures one has to include a global move which changes the spin of a particle (colour of a world line). This move allows fluctuations in the spin and in the square of the total magnetisation $< M_z^2 >$, which is zero only if one simulates in the subspace of zero total magnetisation. However this move is very expensive in CPU time since it is global while the other moves are local.

B Measurements

I have measured the energy and the charge and spin correlation function of the system. The energy can be be decomposed into two parts, E_1 and E_2. To get an estimate for the energy

one has to evaluate the sum

$$\begin{aligned}\langle E_1\rangle &= Z^{-1}\cdot \mathrm{Tr}\left(H_1 e^{-\beta H}\right)\\ &= Z^{-1}\cdot \mathrm{Tr}\left(H_1 (e^{-(\Delta\tau/2)H_1}e^{-\Delta\tau H_2}e^{-(\Delta\tau/2)H_1})^M\right)+\mathrm{O}(\Delta\tau^2)\\ &= Z^{-1}\cdot \mathrm{Tr}\left(H_1 (e^{-\Delta\tau H_1}e^{-\Delta\tau H_2})^M\right)+\mathrm{O}(\Delta\tau^2)\\ &= \sum_{i_1,i_2,\ldots,i_{2M}} P_{i_1,i_2,\ldots,i_{2M}}\frac{\langle i_3|H_1U_1|i_2\rangle}{\langle i_3|U_1|i_2\rangle}+\mathrm{O}(\Delta\tau^2),\end{aligned}$$

where the weight $P_{i_1,i_2,\ldots,i_{2M}}$ of the configuration $(|i_1\rangle,|i_2\rangle,\ldots,|i_{2M}\rangle)$ is given by

$$P_{i_1,i_2,\ldots,i_{2M}} = \frac{\langle i_1|U_1|i_{2M}\rangle\ldots\langle i_2|U_2|i_1\rangle}{\sum_{i_1,i_2,\ldots,i_{2M}}\langle i_1|U_1|i_{2M}\rangle\ldots\langle i_2|U_2|i_1\rangle}\,. \tag{4}$$

In the same way I get

$$\langle E_2\rangle = \sum_{i_1,i_2,\ldots,i_{2M}} P_{i_1,i_2,\ldots,i_{2M}}\frac{\langle i_2|H_2U_2|i_1\rangle}{\langle i_2|U_2|i_1\rangle}+\mathrm{O}(\Delta\tau^2).$$

And for the total energy

$$\begin{aligned}\langle E\rangle &= \langle E_1\rangle+\langle E_2\rangle =\\ &= \sum_{i_1,i_2,\ldots,i_{2M}} P_{i_1,i_2,\ldots,i_{2M}}\left(\frac{\langle i_3|U_1H_1|i_2\rangle}{\langle i_3|U_1|i_2\rangle}+\frac{\langle i_2|U_2H_2|i_1\rangle}{\langle i_2|U_2|i_1\rangle}\right)+\mathrm{O}(\Delta\tau^2)\end{aligned}$$

As the trace is cyclic it does not matter on which Trotter slice I perform the measurements. Averaging over all Trotter slices improves the statistics. The charge-charge correlations are estimated through:

$$\begin{aligned}\langle n_in_j\rangle &= Z^{-1}\cdot \mathrm{Tr}\left(n_in_j e^{-\beta H}\right)\\ &= Z^{-1}\cdot \mathrm{Tr}\left(n_in_j (e^{-(\Delta\tau/2)H_1}e^{-\Delta\tau H_2}e^{-(\Delta\tau/2)H_1})^M\right)+\mathrm{O}(\Delta\tau^2)\\ &= Z^{-1}\cdot \mathrm{Tr}\left(e^{-(\Delta\tau/2)H_1}n_in_je^{-(\Delta\tau/2)H_1}U_2(U_1U_2)^{M-1}\right)+\mathrm{O}(\Delta\tau^2)\\ &= Z^{-1}\cdot \mathrm{Tr}\left((U_1\frac{n_in_j}{2}+\frac{n_in_j}{2}U_1)U_2(U_1U_2)^{M-1}\right)+\mathrm{O}(\Delta\tau^2)\\ &= \sum_{i_1,i_2,\ldots,i_{2M}} P_{i_1,i_2,\ldots,i_{2M}}\frac{\langle i_2|U_1n_in_j+n_in_jU_1|i_1\rangle}{2\langle i_2|U_1|i_1\rangle}+\mathrm{O}(\Delta\tau^2)\end{aligned}$$

and the spin-spin correlations in the same way through

$$\langle S_i^zS_j^z\rangle = \sum_{i_1,i_2,\cdots,i_{2M}} P_{i_1,i_2,\ldots,i_{2M}}\frac{\langle i_2|U_1S_i^zS_j^z+S_i^zS_j^zU_1|i_1\rangle}{2\langle i_2|U_1|i_1\rangle}+\mathrm{O}(\Delta\tau^2).$$

The charge and spin structure factors are defined as the Fourier transforms of the real space correlations:

$$\begin{aligned} S_{ch}(q) &= \sum_x e^{iqx}(n_{i,\uparrow}+n_{i,\downarrow})(n_{i+x,\uparrow}+n_{i+x,\downarrow}), \\ S_{sp}(q) &= \sum_x e^{iqx}(n_{i,\uparrow}-n_{i,\downarrow})(n_{i+x,\uparrow}-n_{i+x,\downarrow}). \end{aligned}$$

Here $n_{j,\uparrow}, n_{j,\downarrow}$ are the particle number operators for particles with spin up (down) at the lattice site j. Due to translation invariance and the cyclicity of the trace measurements can be done at any Trotter slice. Averaging over all these measurements again improves the statistics.

A problem that arises here is that the Metropolis algorithm requires the weights $P_{i_1,i_2,\ldots,i_{2M}}$ (4) to be non negative. If the weights of the configuration are not all positive one has to rewrite the measurement:

$$\langle \mathcal{O} \rangle = \frac{\sum_{\vec{i}} P_{\vec{i}} \mathcal{O}_{\vec{i}}}{\sum_{\vec{i}} P_{\vec{i}}} = \frac{\sum_{\vec{i}} |P_{\vec{i}}| \mathcal{S}_{\vec{i}} \mathcal{O}_{\vec{i}}}{\sum_{\vec{i}} |P_{\vec{i}}| \mathcal{S}_{\vec{i}}} = \frac{\langle \mathcal{S} \cdot \mathcal{O} \rangle}{\langle \mathcal{S} \rangle}$$

Here $P_{\vec{i}}$ is the weight of a configuration and $\mathcal{O}_{\vec{i}}$ the value of the observable $\mathcal{O}$ in that configuration. $\mathcal{S}_{\vec{i}}$ is the sign of the weight $P_{\vec{i}}$ of the configuration. Now the weights $|P_{\vec{i}}|$ are positive. But one has to measure the average value of $\langle \mathcal{S} \cdot \mathcal{O} \rangle$ and the average sign $\langle \mathcal{S} \rangle$. By splitting the measurement into the sum over all configurations with positive weight and average value $\langle \mathcal{O} \rangle_+$ and the sum over all configurations with negative weight and average value $\langle \mathcal{O} \rangle_-$ one can measure the quantities as described above and calculate the total value from

$$\langle \mathcal{O} \rangle = \frac{\langle \mathcal{S} \cdot \mathcal{O} \rangle}{\langle \mathcal{S} \rangle} = \frac{1}{2} \left(\langle \mathcal{O} \rangle_+ + \langle \mathcal{O} \rangle_- + \frac{\langle \mathcal{O} \rangle_+ - \langle \mathcal{O} \rangle_-}{\langle \mathcal{S} \rangle} \right). \tag{5}$$

A small average sign leads to numerical problems due to cancellation in the third term on the right hand side.

C Evaluation of the Measurements

In this section I want to sketch the way I performed my simulations. As the measurements take a lot of time (especially the measurements of the structure factors) it is not useful to do measurements after each local upgrade. The spacing between two upgrades was chosen to be larger than the autocorrelation time. More measurements do not improve the statistics very

much as they are not independent. It is better to use the CPU time to do more upgrades than to do more measurements. As the error on the sign is important and measuring the sign takes nearly no CPU time it was measured after every upgrade nevertheless. This results in an improvement of the statistics without using much CPU time. The average and variance of a sample of about 1000 measurements was stored on disk. Separate measurements were done for configurations with negative and positive weight. Following Furukawa and Imada [14] I interpret my measurements as coming from N_s independent simulations with N_a measurements.

Let me denote the mean value of the i-th measurements of the observable X in the j-th simulation by $\tilde{X}_{j,i}$ and the sign at the time of that measurement by $\tilde{S}_{j,i}$. Let

$$\begin{aligned} X_j^+ &= \frac{1}{N_j^+} \sum_{i \text{ with } \tilde{S}_{j,i}=+1} \tilde{X}_{j,i} \\ X_j^- &= \frac{1}{N_j^-} \sum_{i \text{ with } \tilde{S}_{j,i}=-1} \tilde{X}_{j,i} \\ X_j &= \frac{1}{N_s} \sum_{i=1}^{N_a} \tilde{X}_{j,i} \cdot \tilde{S}_{j,i}. \end{aligned}$$

X_j^+ and X_j^- are the average values of the measurements at positive respectively negative sign. N_j^+ and N_j^- are the number of measurements at positive respectively negative sign. The average sign then is

$$S_j = \frac{1}{N_a} \sum_{i=1}^{N_a} \tilde{S}_{j,i}$$

The straightforward way to estimate the average value of the observable and the statistical error is by calculating estimates for the averages at positive and negative sign and an estimate for the average sign:

$$\begin{aligned} X'_+ &= \frac{\sum_{j=1}^{N_s} N_j^+ X_j^+}{\sum_{j=1}^{N_s} N_j^+} = \frac{\sum_{j,i,\tilde{s}_{j,i}=+1} \tilde{X}_{j,i}}{\sum_{j,i,\tilde{s}_{j,i}=+1} 1} \\ X'_+ &= \frac{\sum_{j=1}^{N_s} N_j^- X_j^-}{\sum_{j=1}^{N_s} N_j^-} = \frac{\sum_{j,i,\tilde{s}_{j,i}=-1} \tilde{X}_{j,i}}{\sum_{j,i,\tilde{s}_{j,i}=-1} 1} \\ S' &= \frac{1}{N_s} \sum_{j=1}^{N_s} S_j \\ \Delta X'_+ &= \frac{1}{N_s} \sqrt{\sum_{j=1}^{N_s} (X_j^+ - X'_+)^2} \end{aligned}$$

$$\Delta X'_- = \frac{1}{N_s}\sqrt{\sum_{j=1}^{N_s}(X_j^- - X'_-)^2}$$

$$\Delta S' = \frac{1}{N_s}\sqrt{\sum_{j=1}^{N_s}(S_j - S')^2}$$

Using formula (5) estimates for the observable and the statistical error can be obtained:

$$A' = \frac{1}{2}\left(X'_+X'_- + \frac{X'_+ - X'_-}{S'}\right)$$

$$\Delta A' = \frac{1}{2}\sqrt{\Delta X'^2_+\left(1+\frac{1}{S'}\right)^2 + \Delta X'^2_-\left(1-\frac{1}{S'}\right)^2 + \left(\frac{X'_+ - X_-}{S'^2}\right)^2 \Delta S'^2}.$$

Another method, proposed by Furukawa and Imada [14], is calculating an estimate of the observable from the results of each of the N_s simulations and averaging over all of the simulations thereafter:

$$A = \frac{1}{N_s}\sum_{j=1}^{N_s} A_j \qquad \text{where} \qquad A_j = \frac{X_j}{S_j}$$

The statistical error is then estimated by

$$\Delta A = \frac{1}{N_s}\sqrt{\sum_{j=1}^{N_s}(A_j - A)^2}.$$

Due to correlations in the measurement of X_j and S_j the statistical fluctuations are smaller than before. However these correlations introduce a systematic error. Now I do not calculate $\langle X_j\rangle/\langle S_j\rangle$, but $\langle X_j/S_j\rangle$ which is not the same when the two variables are correlated. Let me denote the expectation value of the average sign S_j by $\overline{S}$ and of the observable X_j by $\overline{X}$. The difference to the expectation value is denoted by $\delta X_j = X_j - \overline{X}$ and $\delta S_j = S_j - \overline{S}$. Then the systematic error is the expectation value

$$\begin{aligned}
\Delta_s A &= \langle \frac{X_j}{S_j} - \frac{\overline{X}}{\overline{S}} \rangle \qquad (6)\\
&= \frac{1}{\overline{S}}\langle \frac{X_j\overline{S} - \overline{X}S_j}{S_j} \rangle \\
&= \frac{1}{\overline{S}}\langle \frac{(\overline{X}+\delta X_j)\overline{S} - \overline{X}(\overline{S}+\delta S_j)}{\overline{S}+\delta S_j} \rangle \\
&= \frac{1}{\overline{S}}\langle \frac{\delta X_j\overline{S} - \overline{X}\delta S_j}{\overline{S}+\delta S_j} \rangle \\
&\approx \frac{1}{\overline{S}^2}\left\langle \left(-\frac{\delta S_j}{\overline{S}} + \mathrm{O}\left(\left(\frac{\delta S_j}{\overline{S}}\right)^3\right)\right)\left(\delta X_j\overline{S} - \overline{X}\delta S_j\right) \right\rangle
\end{aligned}$$

In obtaining the last line I have used the fact that the averages $\langle \delta S_j \rangle$ and $\langle \delta X_j \rangle$ vanish and only terms of even order remain. When $\delta S_j / S << 1$ the second order terms are the leading ones. To get an estimate for the error one has to find a relation between X_j and S_j (δX_j and δS_j). Denote the expectation value of the measurements at positive sign with X_+ and of the measurements at negative sign with X_-. Let $X_\Delta = \frac{X_+ - X_-}{2}$ and $X_0 = \frac{X_+ + X_-}{2}$. Then the expectation value of X_j, given an average sign S_j, is just

$$\hat{X}_j = \frac{1}{2}((1+S_j)X_+ - (1-S_j)X_-) = X_\Delta + S_j X_0$$

The expectation value of δX_j, given a value of δS_j, then is

$$\delta \hat{X}_j = \hat{X}_j - \overline{X} = (X_\Delta + S_j X_0) - (X_\Delta + \overline{S} X_0) = \delta S_j X_0$$

Inserting these relations into equation (6) leads to

$$\begin{aligned} \Delta_s A &\approx \frac{1}{\overline{S}^3} \langle -\delta S_j \left(\delta S_j X_0 \overline{S} - (X_\Delta + \overline{S} X_0) \right) \delta S_j \rangle \\ &= \frac{1}{\overline{S}^3} \langle X_\Delta \delta S_j^2 \rangle \\ &\approx \frac{X_\Delta}{\overline{S}} \frac{\Delta S^2}{\overline{S}^2}, \end{aligned}$$

where $\Delta S^2 = \langle \delta S_j^2 \rangle$ is the variance of the sign. Of course when X_Δ is smaller than the estimated statistical errors on X'_+ and X'_- these errors have to be taken into account to get reliable estimates for the systematic error. When the size of the simulations is taken large enough, such that $\Delta S^2 << \overline{S}^2$ the systematic error is much smaller than the statistical error. Particularly in measuring the correlation functions near the phase boundary this procedure results in smaller statistical errors than the direct method of interpreting all the data as coming from one simulation and estimating the errors with the straight forward method. The error on the charge fluctuations is typically reduced by a factor two to three. Sometimes it is even reduced by an order of magnitude.

D Sources of Systematic Errors

There are some sources of systematic errors in the algorithm. First there is the $O(\Delta\tau^2)$-correction that arises from the path integral formulation. It is of the order $\beta(\Delta\tau)^2 \alpha^r J^s t^{3-s}$

with $0 \leq r \leq s \leq 3$. This error can be eliminated by extrapolating to $\Delta\tau = 0$ at fixed values of J, β and α. I have carried out most of my calculations at $\Delta\tau t = 0.25$. This introduces an error of about 0.4% on the energies. The correction on the structure factors is much smaller. It is smaller than the statistical error bars.

The restriction to the subspace of zero winding number is not a source of errors but just a boundary effect. The boundary conditions imposed on a finite size lattice do not influence the thermodynamic limit.

All the models I have investigated have a $SU(2)$-symmetry. Therefore the expectation value of the total magnetisation $\langle M_z \rangle$ is equal to zero. The square of the total magnetisation $\langle M_z^2 \rangle$ however is not always zero. In order to achieve ergodicity one has to introduce the global move described above, which flips the spin of a particle. But when the ground state is a spin singlet and the temperature is smaller than the gap to a state of higher spin the square of the total magnetisation is nearly zero. Then the global move may be omitted without introducing a large systematic error.

At half band filling and $\alpha = 1/2$ the ground state is dimerised due to frustration [15] and is a spin singlet. However one cannot be sure that the ground state is a spin singlet for all values of the parameters. For the Hubbard model in the limit $U/t \rightarrow \infty$ Ogata and Shiba [16] have shown that for even number of particles the ground state is a spin singlet for a system with periodic or antiperiodic boundary conditions, except for systems with $4n$ (n is an integer) particles and periodic boundary conditions where the ground state is a spin triplet. The same holds for the $t-J$ model at small values of J/t. When $J/t > 2$ the ground state is a spin singlet for all boundary conditions. Omission of the global move introduces only small systematic errors at low temperatures [8]. I expect that the omission of the global move will not change the qualitative picture. At large negative values of α the ground state need not be a spin singlet. In this parameter region one has to include the global move to get reliable results. At small values of α however the ground state should still be a spin singlet.

All the calculations were carried out at finite temperature and without the global move. To get information on the ground state properties an extrapolation to zero temperature ($\beta \rightarrow \infty$) has to be done. This is difficult since increasing the lattice size leads to an

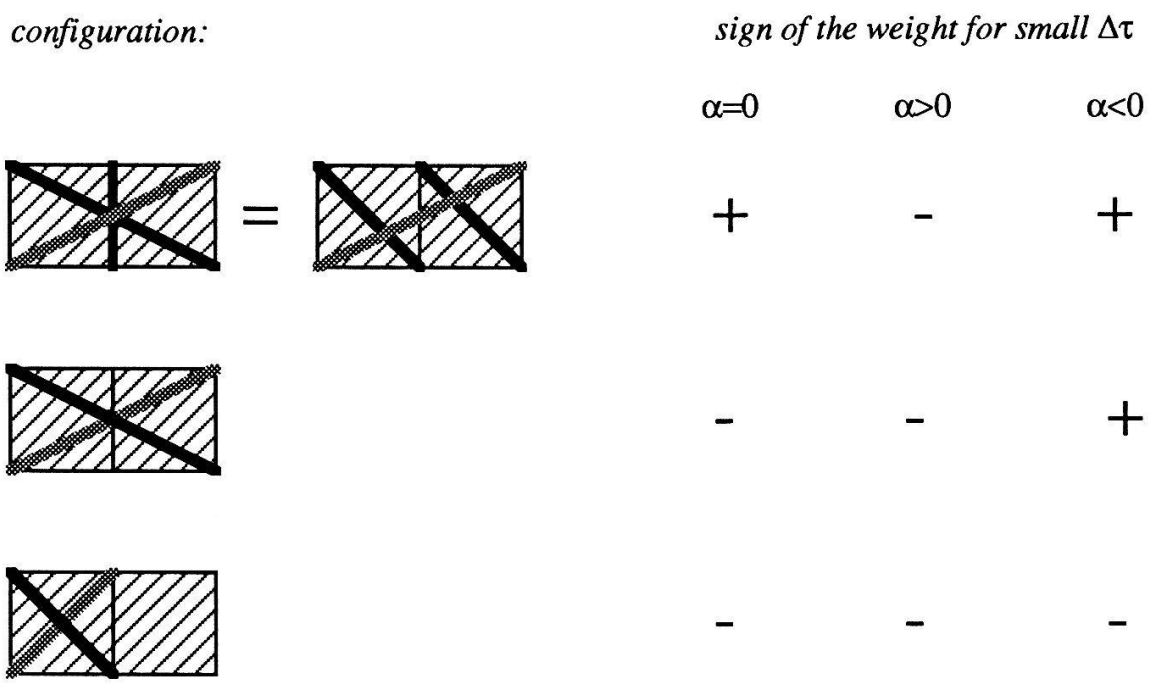

Figure 4a. Local configurations and their sign for different values of α. The two configurations shown in the first row are identical, but there are two ways to connect the sites with worldlines. This has no influence on the calculation, only on the way the configurations are drawn.

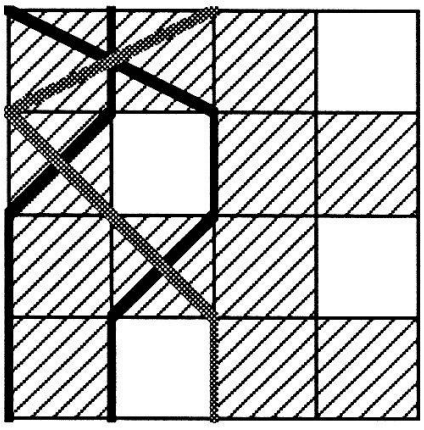

Figure 4b. Periodic configuration with negative overall weight if $\alpha > 0$.

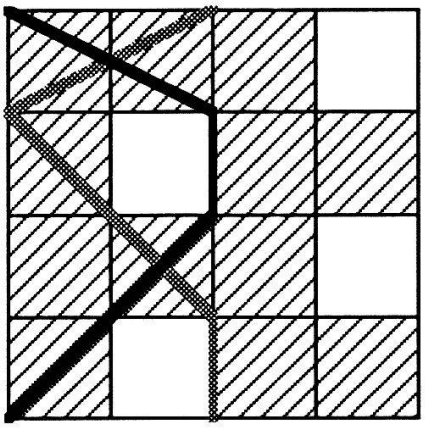

Figure 4c. Periodic configuration with negative overall weight if $\alpha < 0$.

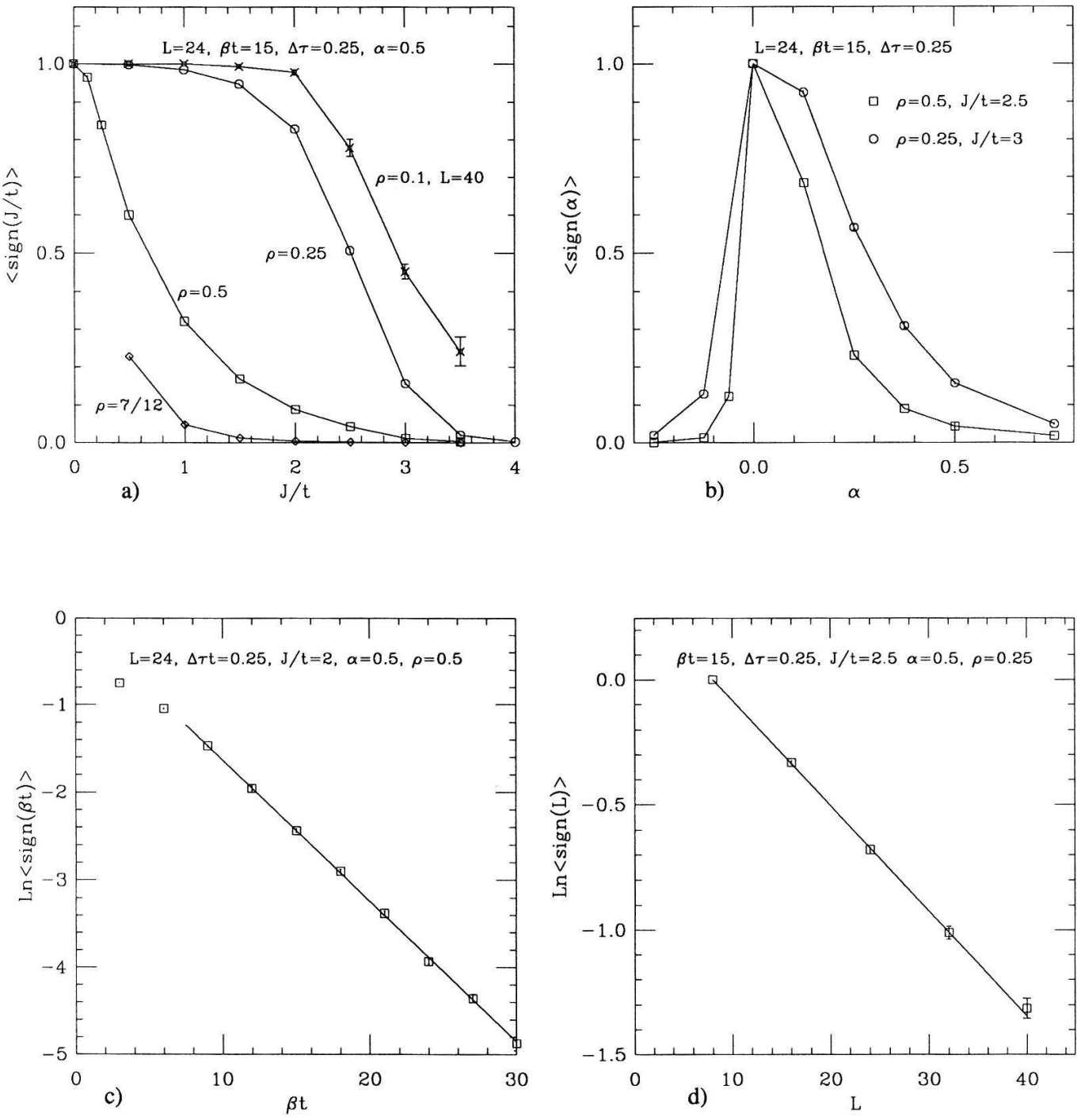

Figure 5. Average sign for different values of the parameters and lattice size. *a)* Dependence on J/t for 14,12 or 6 particles on a lattice of size 24 and for 4 particles on a lattice of size 40. *b)* Dependence on α for 12 particles on 24 sites (ρ=0.5), J/t=2.5 and 6 particles on 24 sites (ρ=0.25), J/t=3.0 . *c)* Dependence on the inverse temperature β for quarter band filling and J/t=2.0 . The solid line is a fit of the values for β>6 to an exponential decrease *d)* Dependence on the lattice size. Here J/t=2.0 and ρ=0.25 . Again the solid line is a fit to an exponential decrease.

exponential decay of the sign, giving rise to numerical problems. I have done most of my calculations at an inverse temperature of $\beta t = 15$. Measurements of the structure factors and real space correlations at lower temperatures give the same results within the error bars.

E The Sign Problem

As mentioned above a small average sign leads to numerical problems in measuring the averages of physical quantities. They arise from the cancellation of terms in the right hand side of equation (5). The sign problem is severe as the average sign decreases exponentially with growing lattice size L and inverse temperature β. This can easily be seen by the following argument. Assume that for a given lattice the probability for a configuration with positive weight is p_+ and for a configuration with negative weight p_-. The average sign will then be $\langle \mathcal{S} \rangle = p_+ - p_-$. Now one doubles the size of the lattice in either direction. If the lattice is large enough the configurations in the two halves are independent and the new probabilities are $p'_+ = p_+p_+ + p_-p_-$ and $p'_- = 2p_+p_-$. The average sign now is $\langle \mathcal{S} \rangle' = p'_+ - p'_- = (p_+ - p_-)^2 = \langle \mathcal{S} \rangle^2$. One sees that the sign decreases exponentially with growing lattice size. This is in accordance with my measurements (figure 5 c,d). There are only small regions of the parameters where one can do Monte Carlo simulations.

In order to get more insight into the sign problem I have looked at the lowest order configurations with a negative weight. In the $t-J$ model there is no sign problem [8]. There the crossing of world lines of opposite spin is the only local configuration with negative weight. But these crossings have to occur in pairs, which gives a positive overall weight. In the $t-J-J'$ model the situation is different. If $J' > 0$ then the crossing of two world lines shown in in the first row of figure 4a has a negative weight, while the same configuration in the $t-J$ model has positive weight. Now we can write down a periodic configuration with negative overall weight (figure 4b). When $J' < 0$ there is a different source of the sign problem. Now the crossing of two world lines that are two lattice sites apart with no world line in between (figure 4a, second row) has positive weight while in the $t-J$ model this configuration has negative weight. In the first case the configuration will have a high acceptance rate in the regions where there is a dense particle rich phase. I expect the sign to be small near half band filling and in the phase separated regime. In the second case one

needs a hole to generate a configuration with negative weight. There will be no sign problem in the case of half band filling. In the region of high density one expects a large sign, while in the region around $\rho = 2/3$ one expects the sign problem to be severe. In the low density region the sign should be larger again.

These qualitative arguments are in good agreement with my measurements. For positive J/t I have been able to perform calculations for small J/t up to the density $\rho = 7/12$. I have been able to simulate in the region of phase separation for densities $\rho \leq 0.25$ only. Even there it is very hard to get quantitative results. In figure 5a I have plotted the dependence of the sign on J/t for several band fillings. For $J'/t < 0$ it is possible to simulate in the high and low density regions. When the absolute value of J'/t is much larger than J/t we have a large next nearest neighbour Heisenberg coupling and only a very small nearest neighbour interaction. The acceptance rate for the above configurations is then very small and there should be no sign problem. Figure 5b shows the dependence of the average sign on α for two parameter regions.

III Results

A Comparison with the Checkerboard Decomposition and Exactly Solvable Models

I have compared the results of my algorithm with exact calculations and the checkerboard decomposition for some exactly solvable systems. I have simulated the Heisenberg model, free electrons and the supersymmetric $t-J$ model(see figures 6a,b,c). My simulations agree favourably with results of Assaad and Würtz [8] obtained with the checkerboard decomposition and with the exact ground state energies. The small deviations from the ground state energies can be explained as finite temperature and boundary effects.

One sees that the $(\Delta\tau)^2$-correction is much smaller than with the checkerboard decomposition. Given a tolerance for the systematic error (produced by a finite value of $\Delta\tau$) a higher value of $\Delta\tau$ may be chosen. This results in smaller lattices. The acceptance rate grows as a function of $\Delta\tau$. A higher acceptance rate results in shorter autocorrelation times

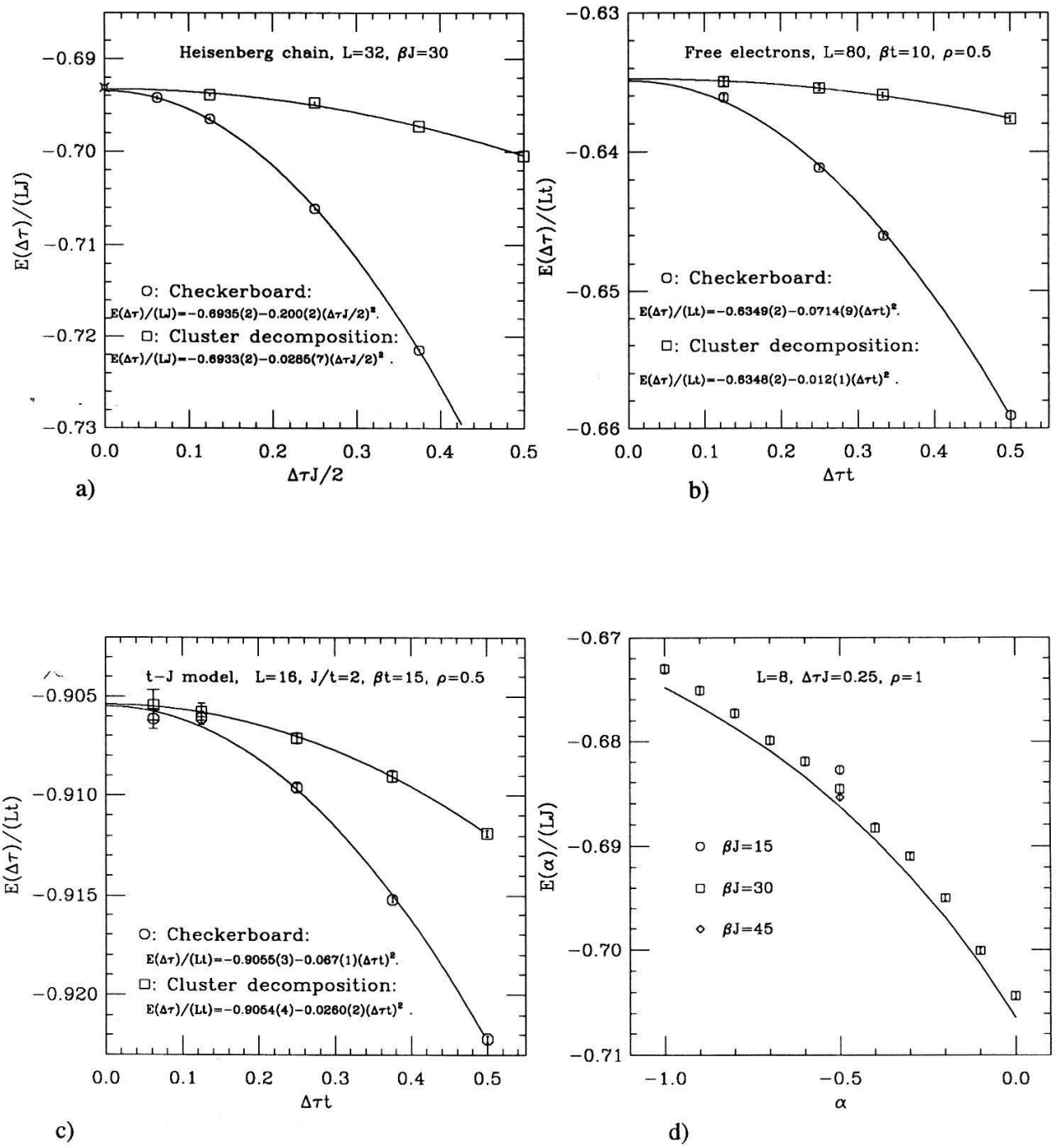

Figure 6. Comparison of exact results with results of the cluster decomposition and the checkerboard decomposition. *a,b,c)* Energy per site in the Heisenberg model (lattice size L=32, βJ=30), free electrons (lattice size L=80, βt=15) and the supersymmetric t-J model (lattice size L=16, βt=15). Plotted are the energies for different values of $\Delta\tau$ and the quadratic extrapolation to $\Delta\tau$=0. *d)* Energy per site in the Heisenberg model on a lattice with eight sites and a next nearest neighbour coupling with strength $J'=\alpha J$, for different values of α. The solid lines are the exact ground state energies calculated for periodic boundary conditions (see [Majumdar 1969]).

and therefore shorter simulations. As expected from the Feynman path integral formulation, the extrapolation to $\Delta\tau = 0$ is independent of the special type of decomposition. Another advantage of the method is that it can be used for models with next nearest neighbour interactions and double layers.

I have also compared the method with exact results by Majumdar and Ghosh [15] for the antiferromagnetic Heisenberg model with next nearest neighbour interaction (figure 6d). The results are in good agreement for $\alpha \leq 0$. The deviations, less than one percent, are smaller than the temperature. They can be explained as finite temperature and boundary effects. At this band filling it is not possible to simulate the region $\alpha > 0$ due to the sign problem.

B Simulation of the $t - J - J'$ model, $\alpha > 0$

Here I describe the results of my calculations and compare them to the $t - J$ model. The results for the $t - J$ model are taken from Assaad and Würtz [8].

B.1 Low values of J/t

In the limit $J/t \to 0$ the $t - J$ model is the large-U limit of the Hubbard model. When $J = J' = 0$ the hopping term produces a $4k_f$ charge density wave ($k_f = \rho\pi/2$). As there is no spin interaction the state is degenerate in the spin degrees of freedom. Introducing a small spin interaction J lifts this degeneracy and produces a $2k_f$ spin density wave. This is exactly what is expected since the $t - J$ models scales to a Luttinger liquid in the limit of small J/t. It is also confirmed by results of Ogata et al. [9] and Assaad and Würtz [8]. In the $t - J - J'$ model I see the same structures at low values of J/t. There is a peak in the charge structure factor at $q = 4k_f$ (figures 7a, 8a) and a peak at $q = 2k_f$ in the spin structure factor (figures 7b, 8b, 9b). They correspond to a $4k_f$ charge density wave and a $2k_f$ spin density wave. These density waves can also be seen in the real space correlations (figure 7c,d). The spin and charge structures at a density of $\rho = 7/12$ (14 particles on 24 sites) show the same features as the structures at lower densities. It is not possible to simulate at higher densities due to the sign problem.

The $t - J$ model loses this Hubbard like character at higher values of J/t. The spin

interaction is in competition with the hopping term as it favours antiferromagnetic alignment of particles on nearest neighbour sites. The particles will tend to form nearest neighbour pairs. The $4k_f$ charge peak vanishes and is replaced by a peak at $q = 2k_f$. The $2k_f$ spin peak vanishes also and there is a maximum at $q = \pi$ in the spin structure factor, corresponding to antiferromagnetic alignment of spins on nearest neighbour sites.

In the $t - J - J'$ model ($J' = J/2$) there are similar changes at higher values of J/t. At quarter band filling the $2k_f$ spin density wave and the $4k_f$ charge density wave correspond to the structure $\uparrow$. $\downarrow$. $\uparrow$. $\downarrow$. (arrows denote up and down spins, dots denote holes). This structure is also favoured by the antiferromagnetic next nearest neighbour coupling J'. Therefore J' enhances this structure. When increasing J/t it does not break down as soon as in the $t - J$ model. Even at $J/t = 2.5$ where there is no $4k_f$ charge peak in the $t - J$ model any more, it is still more pronounced than the $2k_f$ charge structure (figures 7a,b). At even higher values of J/t these structures vanish nevertheless and we see the same behaviour as at lower densities ($J/t = 3$ in figures 7a,b). The same behaviour can be observed at the slightly higher band filling of $\rho = 7/12$.

At $J/t = 2.5$ and quarter band filling I have looked at the dependence of the charge and spin structures on the relative strength of the next nearest neighbour coupling $\alpha = J'/J$ (figure 11). In the $t - J$ model ($\alpha = 0$) there is no $4k_f$ charge peak and no $2k_f$ spin peak at this value of J/t. Instead there is a $2k_f$ peak in the charge structure factor and a maximum at $q = \pi$ in the spin structure factor. With growing α these structures change continuously to the structures of the $t - J - J'$ model with $J' = J/2$. A $4k_f$ charge density wave and a $2k_f$ spin density wave is formed and these structures become more dominant at higher values of α. At small negative values of α the $2k_f$ charge density wave is enhanced and the $4k_f$ contribution suppressed.

At lower densities the $4k_f$ charge and $2k_f$ spin structures are not enhanced as much by the next nearest neighbour coupling. They vanish at much smaller values of J/t (figures 8a,b; 9). But due to the next nearest neighbour interaction the particles tend to align antiferromagnetically on nearest neighbour and next nearest neighbour sites. This results in a maximum in the spin structure factor not at $q = \pi$ but at lower values of q (figures 8b, 9b). With growing J/t the maximum moves to higher wave vectors q, corresponding to a

higher proportion of nearest neighbour pairs.

At a certain density dependent value of J/t one can see the onset of phase separation.

B.2 Phase Separation

According to results of Ogata [17] phase separation occurs at $J/t = 3.4$ for $\rho = 0.5$ and $J/t = 2.2$ for $\rho = 0.25$. At quarter band filling I am not able to observe the phase separation due to sign problem, but at lower densities I can simulate in the region of phase separation. At a band filling of $\rho = 0.25$ and $J/t = 2.0$ the system is not yet phase separated, but at $J/t = 2.5$ the onset of phase separation can be seen. The long wavelength charge structures grow rapidly in this region. The same can be observed at a band filling of $\rho = 0.1$ between $J/t = 1.5$ and $J/t = 2.0$. These observation are consistent with the values for the phase separation obtained by Ogata.

It is of interest to investigate the nature of the phase separated state. In the limit $J/t \rightarrow \infty$ the system will be separated into a dimerised chain of electrons and a sea of holes. But the system does not look like this in the region near phase separation. In the $t - V$ model the system is separated in an island of particles and a sea of holes immediately after phase separation. In the $t - J$ model there is a small region at low densities where the particle rich phase can be caricatured as a gas of nearest neighbour singlet pairs. When J/t becomes larger than 3.5 the system is totally phase separated into a Heisenberg chain and a sea of holes.

In the $t - J - J'$ model I have been able to simulate in the phase separated region at low densities ($\rho \leq 0.25$) only. Near the phase transition the system is not yet totally phase separated, but the particle rich phase can be caricatured as a gas of nearest neighbour and next nearest neighbour singlet pairs. I have done a least square fit of the spin structure factor to the structure factor of such a gas:

$$S_{spin}^{fit} = a \cdot 2\rho(1 - \cos(q)) + b \cdot 2\rho(1 - \cos(q/2)). \tag{7}$$

The first term on the right hand side is the spin structure factor of a gas of nearest neighbour bound pairs and the second term the structure factor of a gas of next nearest neighbour pairs. The fit is included in the spin structure factor in figures 8b, 9b (for $\rho = 0.25, J/t = 3.0$ and

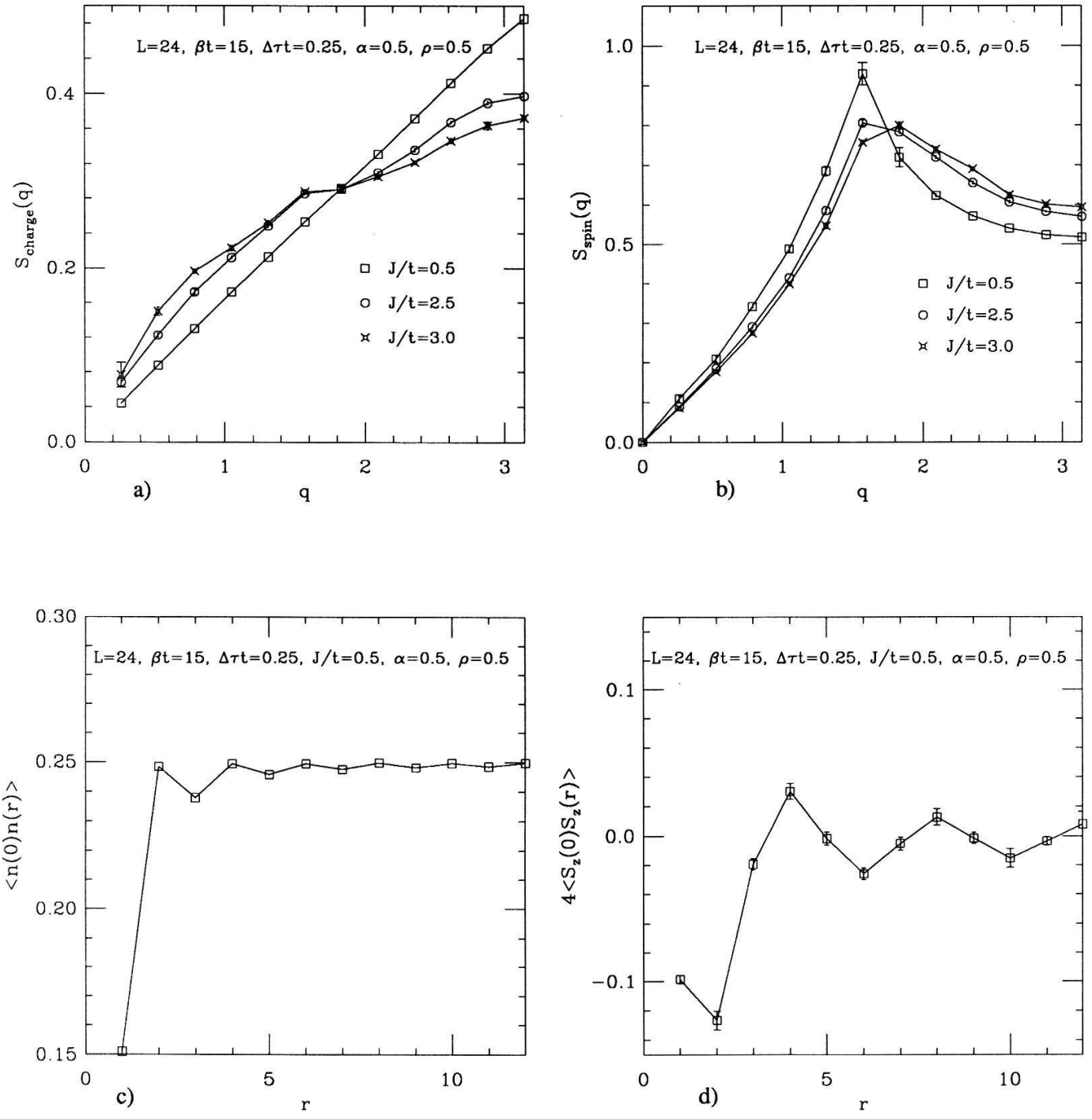

Figure 7. Structure factors and correlations for quarter band filling (12 particles on 24 sites). The temperature is βt=15, the next nearest neighbour coupling is $J'=J/2$. *a,b)* Charge and spin structure factors for J/t=0.5, 2.5, 3.0 . *c,d)* Real space chargeand spin correlations for J/t=0.5. The spin and charge density waves can clearly be seen.

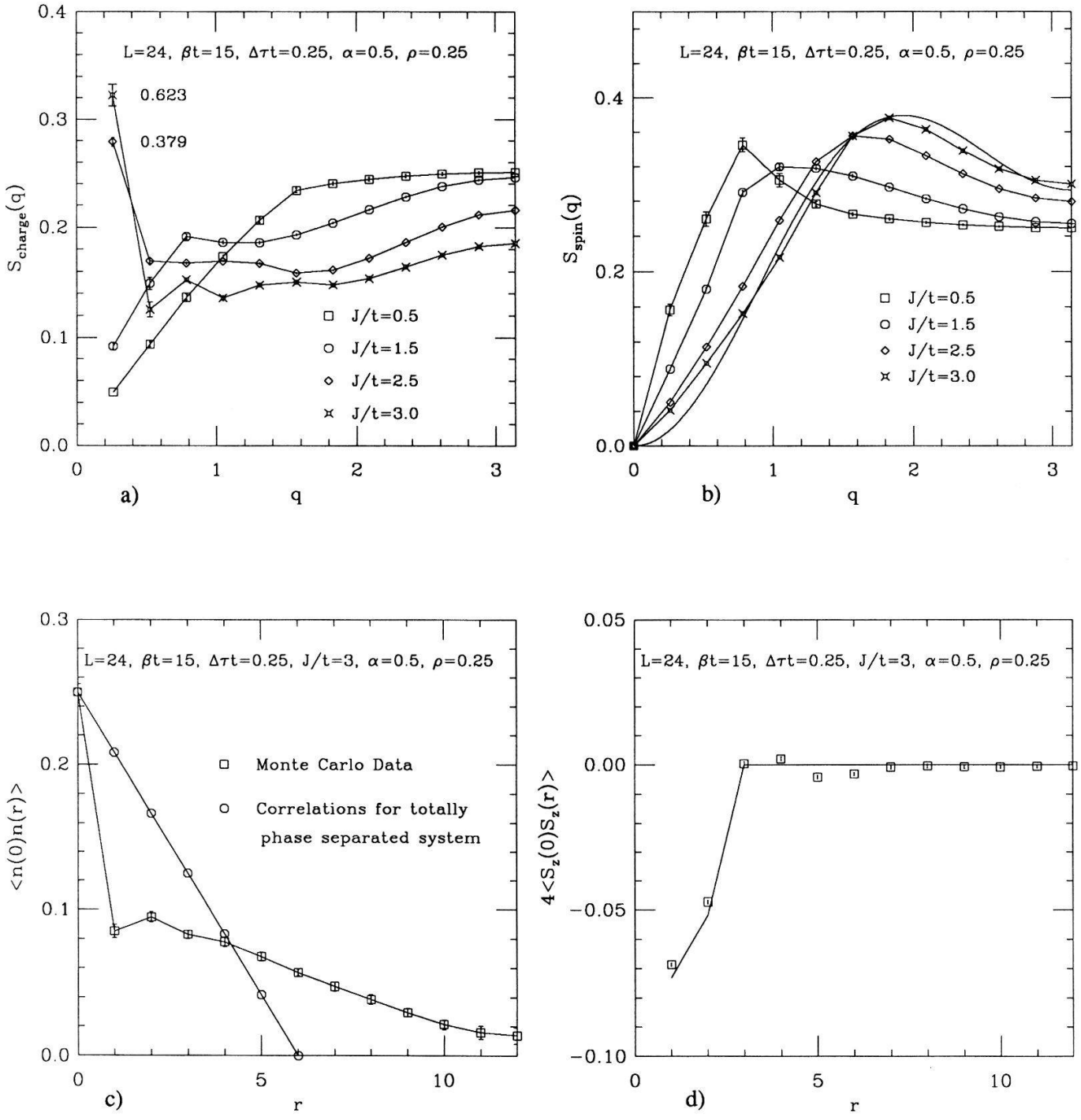

Figure 8. Structure factors and correlations for 6 particles on 24 sites. The temperature is βt=15, the next nearest neighbour coupling is $J'=J/2$. *a,b)* Charge and spin structure factors for J/t=0.5, 1.5, 2.5, 3.0 . The solid line in the spin structure factor is a least square fit of the data for J/t=3.0 to the structure factor of a gas of next neighbour and next nearest neighbour bound pairs. *c,d)* Real space charge and spin correlations for J/t=3.0 . The charge correlations are compared to the correlations for the totally phase separated system. The solid line in the spin structure factors is the same fit as in figure *b*.

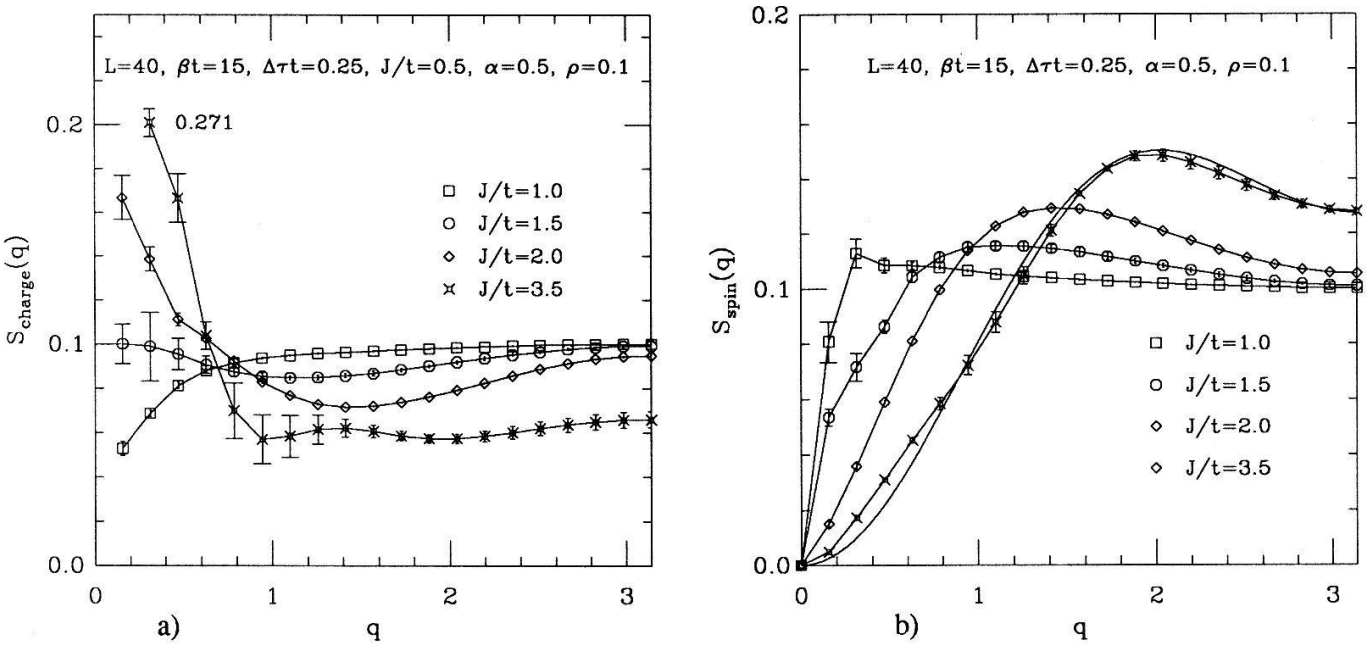

Figure 9 Structure factors and real space correlations for 4 particles on a lattice of 40 sites. The temperature is $\beta t=15$, the next nearest neighbour coupling is $J'=J/2$. The solid line in figure *b)* is again a fit to the structure factor of a gas of next neighbour and next nearest neighbour bound pairs.

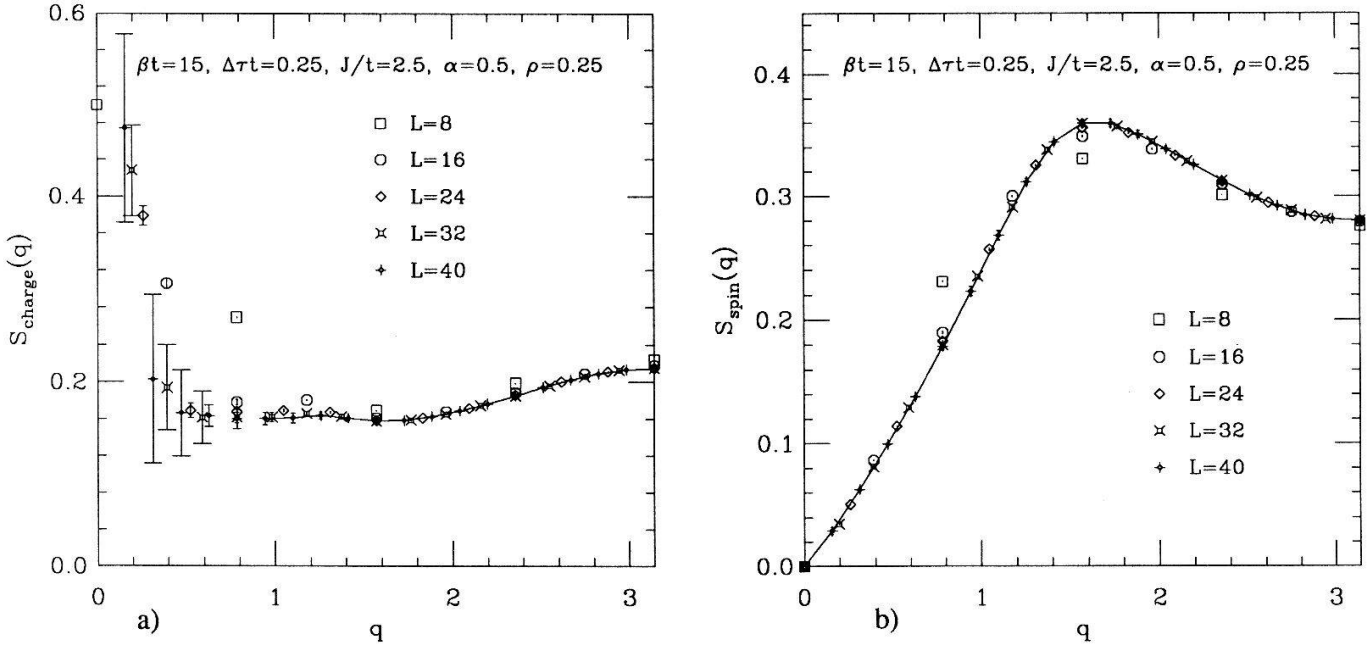

Figure 10. Charge and spin structure factors and real space correlations for a band filling of $\rho=0.25$ on lattices of different sizes. $J/t=2.5$ and $J'=J/2$. The lattice sizes range from $L=8$ to $L=40$ sites.

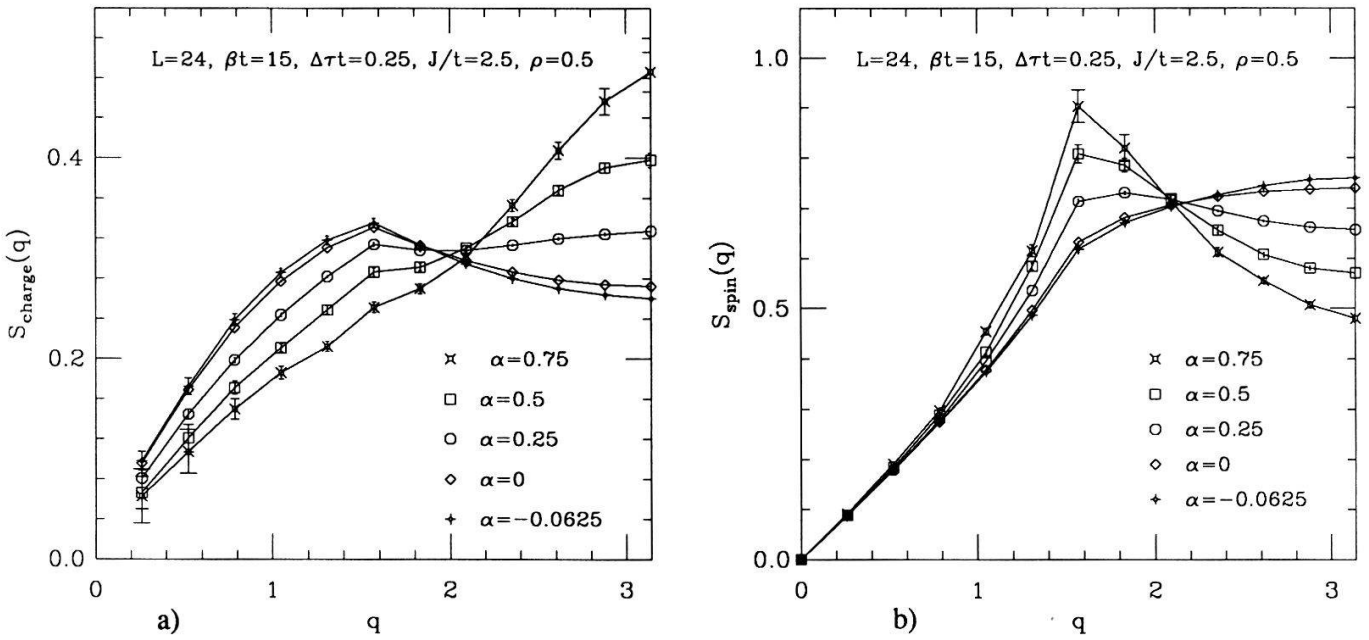

Figure 11. Charge and spin structure factors for different values of the next nearest neighbour coupling $J'=\alpha J$ at quarter band filling. α ranges from small negative values to $\alpha=0.75$. At $\alpha = 0$ the *t-J-J'* model reduces to the *t-J* model.

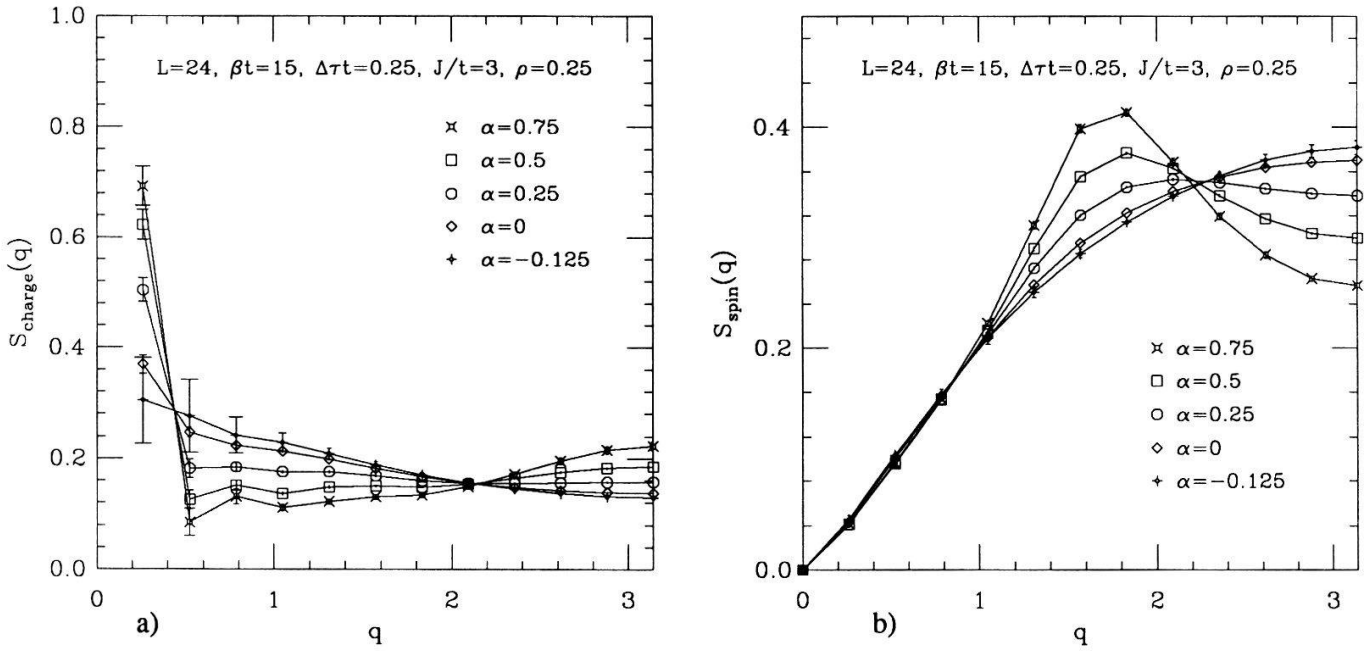

Figure 12. Charge and spin structure factors for different values of the next nearest neighbour coupling $J'=\alpha J$ for 6 particles on 24 sites. α ranges from small negative values to $\alpha=0.75$. At $\alpha = 0$ the *t-J-J'* model reduces to the *t-J* model.

$\rho = 0.1, J/t = 3.5$) and in the real space spin correlation in figure 8d ($\rho = 0.25, J/t = 3.0$). With growing J/t nearest neighbour pairs are preferred over next nearest neighbour ones. This results in a shift to the right of the maximum in the spin structure factor (figure 8b,9b). It is consistent with the expectation of a dimerised Heisenberg chain in the limit $J/t \rightarrow \infty$.

The fact that the system is not yet fully phase separated can be seen from figure 8c, where I have shown the real space charge correlation and compared them to the charge correlations of a totally phase separated system. There are still holes in the particle rich phase. This is also evident from the charge structure factors (figure 8b,9b). If the particle rich phase were a Heisenberg chain without holes the charge structure factor would be zero at $q = \pi$. The nonzero charge structure factor at $q = \pi$ (see figure 8a,9a) arises from local modulations of the charge density (it corresponds to the structure $particle - hole - particle - hole$).

At $\rho = 0.25$ and $J/t = 3.0$ I have again investigated the dependence of the structure factors on the relative strength of the next nearest neighbour coupling α (figure 12). At $\alpha = 0$ the $t - J - J'$ model is just the $t - J$ model and the system can be caricatured as a gas of singlet bound pairs. With growing $J' = \alpha J$ more and more next nearest neighbour pairs are formed. Again the structure factors evolve continuously and there is no indication of any phase transition.

B.3 Finite Size Scaling

I have done a finite size scaling analysis at $\rho = 0.25$ and $J/t = 2.5$, which is in the phase separated region (figure 10). The maximum in the spin structure factor gets more pronounced with growing lattice size. Therefore I expect it to be present in the thermodynamic limit. The charge structure peak at small wavelengths remains as well. The maximum at $q = \pi$ in the charge structure factor does not scale to zero but remains finite. I conclude that the above description of the ground state near the phase separation is valid in the thermodynamic limit. A lattice size of $L = 24$ seems to be sufficient to get a qualitative picture of the structure factors. For quantitative results one has to go to larger lattices, but a lattice size of $L = 24$ seems to be sufficient to see the qualitative structure. To get reliable values for the long range correlations one has to simulate lattices much larger than the correlation distance considered. A larger lattice size results in longer autocorrelation time for the Monte Carlo

process and in a smaller sign. This makes it very hard to get any quantitative results such as the critical exponents from the Monte Carlo data.

B.4 Scaling to the Tomonaga-Luttinger Liquid

The Hubbard model and the $t-J$ model at $J/t \to 0$ and $J/t = 2$ scale to the Tomonaga Luttinger fixedpoint. As the structure factors vary continuously with J/t and $\alpha = J'/J$ one can expect that the $t-J-J'$ model scales to the same fixedpoint if there is no phase boundary and no spin gap opens. In my simulations I see no indication of such a phenomena. In a Tomonaga-Luttinger liquid the real space correlations show a power law decay. The critical exponents may be calculated from a dimensionless K_ρ:

$$\begin{aligned} \langle n(r)n(0)\rangle &\sim A_0 r^{-2} + A_1 \cos(2k_f r)\, r^{-(1+K_\rho)} + A_2 \cos(4k_f r)\, r^{-4K_\rho}, \\ \langle S_z(r)S_z(0)\rangle &\sim B_0\, r^{-2} + B_1 \cos(2k_f r)\, r^{-(1+K_\rho)}, \end{aligned}$$

where $r >> 1$. Logarithmic corrections have been omitted in the above equations. In the $U \to \infty$ Hubbard model $K_\rho = 0.5$ independent of the band filling. The same holds in the $J/t \to 0$ limit of the $t-J$ model. My results are consistent with these relations. They indicate an increase of K_ρ with J/t. Phase separation occurs when the compressibility v_c/K_ρ goes to zero [9]. Beyond phase separation the system is no longer a Tomonaga-Luttinger liquid. The increase of the $2k_f$ spin structure and $4k_f$ charge structure with growing J' at quarter band filling and $J/t = 2.5$ (figure 11) indicates that there K_ρ decreases with the next nearest neighbour coupling J'. These observations as well as the values of J/t where phase separation occurs are consistent with calculations of K_ρ from the energies of the ground state and the first few excited states, done by Ogata [17].

C Simulation of the $t-J-J'$ model, $\alpha < 0$

At negative α one has to be very careful when omitting the global move as the ground state need not be not a spin singlet at large negative values of α. At small absolute values of α however one can still expect to get qualitatively correct results. At half band filling I have compared my results to the exact results of Majumdar and Ghosh [15] for a lattice of eight sites. As mentioned above the energies are consistent with their results. They have also

shown that the ground state is a spin singlet for $-1 \leq \alpha \leq 1$. Therefore the global move may be omitted. My calculations show that the peak in the spin structure factor at $q = \pi$ gets more pronounced with growing negative α, compared to the Heisenberg model ($\alpha = 0$). This is what one expects since the ferromagnetic next nearest neighbour coupling favours the structure of alternating spins.

IV Conclusion

I have investigated the one-dimensional $t - J - J'$ model with the quantum Monte Carlo world line algorithm. Due to frustration there is a minus sign problem which makes simulations impossible in parameter regions with large frustration. As the average sign decreases exponentially with growing lattice size it is difficult to obtain information on the thermodynamic limit (lattice size $L \rightarrow \infty$) and on the ground state properties (inverse temperature $\beta \rightarrow \infty$). A small average sign leads to cancellations. However there are some regions where simulations can be done and qualitative information obtained. As the sign problem arises in very small systems (e.g. four sites and small β at half band filling) this is a good model to investigate the sign problem. Measurements of the sign confirm that it decreases exponentially with the lattice size.

The $t - J - J'$ model ($J/t > 0, J' = J/2$) cannot be simulated at half band filling due to the sign problem. At this filling the ground state is dimerised into singlet singlet pairs and there is a spin gap [15]. At the densities where I could carry out my simulations there is no indication of a spin gap any more, but there might still be a spin gap at higher densities.

Around quarter band filling the system can be simulated for low values of J/t. The spin and charge structure show qualitatively the same behaviour as in the $t - J$ model. They seem to change continuously with J/t and $\alpha = J'/J$. It is reasonable to expect that the model scales to the Tomonaga-Luttinger fixedpoint. At lower band fillings the system shows the same behaviour. There it is possible to simulate in the phase separated region as well. In the limit $J/t \rightarrow \infty$ the system is separated into a dimerised Heisenberg chain and a sea of holes. At lower values of J/t it is not yet fully phase separated but, similar to the $t - J$ model, the particle rich phase still contains some holes. It can be caricatured as a gas of

nearest neighbour and next nearest neighbour singlet pairs. This description still holds for $J/t \geq 3.5$ where the $t-J$ model is already completely phase separated.

In order to simulate the $t-J-J'$ model I have looked for a new decomposition of the Hamiltonian. This decomposition can then be used with the transfer matrix method or the world line algorithm. It allows simulations of one-dimensional systems with nearest neighbour and next nearest neighbour interactions. When one includes next nearest neighbour interactions the system may be frustrated, giving rise to a minus sign problem. This decomposition into four particle terms is also of advantage when simulating systems with nearest neighbour interactions only. The exact solution of a four particle system, in comparison with the two particle system in the checkerboard decomposition, results in a smaller systematic error arising from the Trotter decomposition. Furthermore the decomposition can be used to simulate one-dimensional double layers.

Acknowledgements

I wish to thank Prof. T. M. Rice and D. Würtz for giving me the opportunity of carrying out this work. I am equally grateful for stimulating conversations with F. F. Assaad and M. Ogata. I want to thank M. Borer for his system support on the IBM 3090 at the ETH Zürich.

Appendix: The Matrix Elements.

The matrices H_1, H_2, U_1, U_2 are in block-diagonal form. They consist of identical blocks $H_{(i)}$ respectively $\exp(H_i)$. The matrix $H_{(i)}$ again splits into smaller matrices in the subspaces of constant particle number and magnetisation. The diagonalisation of these matrices was done numerically and the matrix elements stored in a file that was read by the simulation programme. The advantage then is that one does not have to change the programme to simulate a different model, but has to change the file of matrix elements only.

I got the matrix elements of $H_{(i)}$ from the relations

$$\begin{aligned}
-th_k^\dagger h_{k+1} \quad & |\sigma,0\rangle && = && -t|0,\sigma\rangle \\
-th_k^\dagger h_{k+1} \quad & |\sigma,\pm\sigma\rangle && = && 0 \\
-th_k^\dagger h_{k+1} \quad & |0,0\rangle && = && 0 \\
J(\vec{S}_i\vec{S}_{i+1}-\tfrac{1}{4}n_in_{i+1}) \quad & |\sigma,-\sigma\rangle && = && \tfrac{J}{2}|\sigma,-\sigma\rangle+\tfrac{J}{2}|-\sigma,\sigma\rangle \\
J(\vec{S}_i\vec{S}_{i+1}-\tfrac{1}{4}n_in_{i+1}) \quad & |\sigma,\sigma\rangle && = && 0 \\
J(\vec{S}_i\vec{S}_{i+1}-\tfrac{1}{4}n_in_{i+1}) \quad & |\sigma,0\rangle && = && 0 \\
J(\vec{S}_i\vec{S}_{i+1}-\tfrac{1}{4}n_in_{i+1}) \quad & |0,\sigma\rangle && = && 0 \\
J(\vec{S}_i\vec{S}_{i+1}-\tfrac{1}{4}n_in_{i+1}) \quad & |0,0\rangle && = && 0 \\
\alpha J(\vec{S}_i\vec{S}_{i+1}-\tfrac{1}{4}n_in_{i+1}) \quad & |\sigma,\cdot,-\sigma\rangle && = && \tfrac{\alpha J}{2}|\sigma,\cdot,-\sigma\rangle+\tfrac{\alpha J}{2}|-\sigma,\cdot,\sigma\rangle \\
\alpha J(\vec{S}_i\vec{S}_{i+2}-\tfrac{1}{4}n_in_{i+2}) \quad & |\sigma,\cdot,\sigma\rangle && = && 0 \\
-\alpha J(\vec{S}_i\vec{S}_{i+2}-\tfrac{1}{4}n_in_{i+2}) \quad & |\sigma,\cdot,0\rangle && = && 0 \\
-\alpha J(\vec{S}_i\vec{S}_{i+2}-\tfrac{1}{4}n_in_{i+2}) \quad & |0,\cdot,\sigma\rangle && = && 0 \\
-\alpha J(\vec{S}_i\vec{S}_{i+2}-\tfrac{1}{4}n_in_{i+2}) \quad & |0,\cdot,0\rangle && = && 0.
\end{aligned}$$

The ket $|.,.\rangle$ describes the states on the sites i and $i+1$ and the ket $|.,.,.\rangle$ the states on the sites i, $i+1$ and $i+2$. A 0 denotes an empty site, a $\cdot$ any state and a σ a particle with z-component of spin σ. The matrix is block diagonal and the invariant subspaces are the subspaces with constant particle number n and constant spin. In the following the ket $|.,.,.,.\rangle$ denotes the state on four neighbouring sites in the chain. The calculations were done separately in each of the following subspaces:

- $n=0$ or $n=4, S^z=\pm 2$

  This case is trivial as the subspaces are one-dimensional and the energy of these states is zero.

- $n=1, S^z=\pm\frac{1}{2}$ or $n=3, S^z=\pm\frac{3}{2}$

  In this case I used the basis

$$\{|\sigma,0,0,0\rangle,|0,\sigma,0,0\rangle,|0,0,\sigma,0\rangle,|0,0,0,\sigma\rangle\} \qquad \text{respectively}$$
$$\{|0,\sigma,\sigma,\sigma\rangle,|\sigma,0,\sigma,\sigma\rangle,|\sigma,\sigma,0,\sigma\rangle,|\sigma,\sigma,\sigma,0\rangle\}$$

and the matrix is

$$\begin{pmatrix} 0 & -\frac{t}{2} & 0 & 0 \\ -\frac{t}{2} & 0 & -t & 0 \\ 0 & -t & 0 & -\frac{t}{2} \\ 0 & 0 & -\frac{t}{2} & 0 \end{pmatrix}$$

- $n = 2$, spin triplet

  In this case no spin flip can occur. I used the basis

  $$\{|\sigma,\sigma',0,0\rangle, |\sigma,0,\sigma',0\rangle, |\sigma,0,0,\sigma'\rangle, |0,\sigma,\sigma',0\rangle, |0,\sigma,0,\sigma'\rangle, |0,0,\sigma,\sigma'\rangle\},$$

  where the two spins σ and σ' are in triplet state. The matrix is

  $$\begin{pmatrix} 0 & -t & 0 & 0 & 0 & 0 \\ -t & 0 & -\frac{t}{2} & -\frac{t}{2} & 0 & 0 \\ 0 & -\frac{t}{2} & 0 & 0 & -\frac{t}{2} & 0 \\ 0 & -\frac{t}{2} & 0 & 0 & -\frac{t}{2} & 0 \\ 0 & 0 & -\frac{t}{2} & -\frac{t}{2} & 0 & -t \\ 0 & 0 & 0 & 0 & -t & 0 \end{pmatrix}$$

- $n = 2$, spin singlet

  In this case I take the same basis as before, but now the two spins are in singlet state. The matrix is

  $$\begin{pmatrix} -\frac{J}{2} & -t & 0 & 0 & 0 & 0 \\ -t & -\alpha J & -\frac{t}{2} & -\frac{t}{2} & 0 & 0 \\ 0 & -\frac{t}{2} & 0 & 0 & -\frac{t}{2} & 0 \\ 0 & -\frac{t}{2} & 0 & -J & -\frac{t}{2} & 0 \\ 0 & 0 & -\frac{t}{2} & -\frac{t}{2} & -\alpha J & -t \\ 0 & 0 & 0 & 0 & -t & -\frac{J}{2} \end{pmatrix}$$

- $n = 3$, $S^z = \pm\frac{1}{2}$

  In this case the matrix is the biggest one, of size 12×12. I used the basis

  $$\{|\sigma,\sigma,-\sigma,0\rangle, |\sigma,-\sigma,\sigma,0\rangle, |-\sigma,\sigma,\sigma,0\rangle,$$
  $$|\sigma,\sigma,0,-\sigma\rangle, |\sigma,-\sigma,0,\sigma\rangle, |-\sigma,\sigma,0,\sigma\rangle,$$
  $$|\sigma,0,\sigma,-\sigma\rangle, |\sigma,0,-\sigma,\sigma\rangle, |-\sigma,0,\sigma,\sigma\rangle,$$
  $$|0,\sigma,\sigma,-\sigma\rangle, |0,\sigma,-\sigma,\sigma\rangle, |0,-\sigma,\sigma,\sigma\rangle\}$$

and the matrix is

$$\begin{pmatrix}
\frac{-J\mu}{2} & \frac{J}{2} & \frac{\alpha J}{2} & \frac{-t}{2} & 0 & 0 & 0 & 0 & 0 & 0 & 0 & 0 \\
\frac{J}{2} & \frac{-3J}{4} & \frac{J}{4} & 0 & \frac{-t}{2} & 0 & 0 & 0 & 0 & 0 & 0 & 0 \\
\frac{\alpha J}{2} & \frac{J}{4} & -\frac{J\nu}{4} & 0 & 0 & \frac{-t}{2} & 0 & 0 & 0 & 0 & 0 & 0 \\
\frac{-t}{2} & 0 & 0 & \frac{-\alpha J}{2} & \frac{\alpha J}{2} & 0 & -t & 0 & 0 & 0 & 0 & 0 \\
0 & \frac{-t}{2} & 0 & \frac{\alpha J}{2} & \frac{-J\nu}{4} & \frac{J}{4} & 0 & -t & 0 & 0 & 0 & 0 \\
0 & 0 & \frac{-t}{2} & 0 & \frac{J}{4} & \frac{-J}{4} & 0 & 0 & -t & 0 & 0 & 0 \\
0 & 0 & 0 & -t & 0 & 0 & \frac{-J}{4} & \frac{J}{4} & 0 & \frac{-t}{2} & 0 & 0 \\
0 & 0 & 0 & 0 & -t & 0 & \frac{J}{4} & \frac{-J\nu}{4} & \frac{\alpha J}{2} & 0 & \frac{-t}{2} & 0 \\
0 & 0 & 0 & 0 & 0 & -t & 0 & \frac{\alpha J}{2} & \frac{-\alpha J}{2} & 0 & 0 & \frac{-t}{2} \\
0 & 0 & 0 & 0 & 0 & 0 & \frac{-t}{2} & 0 & 0 & \frac{-J\nu}{4} & \frac{J}{4} & \frac{\alpha J}{2} \\
0 & 0 & 0 & 0 & 0 & 0 & 0 & \frac{-t}{2} & 0 & \frac{J}{4} & \frac{-3J}{4} & \frac{J}{2} \\
0 & 0 & 0 & 0 & 0 & 0 & 0 & 0 & \frac{-t}{2} & \frac{\alpha J}{2} & \frac{J}{2} & \frac{-J\mu}{2}
\end{pmatrix}$$

where $\mu = \alpha + 1$ and $\nu = 2\alpha + 1$.

- $n = 4$ $S^z = \pm 1$

Here I used the basis

$$\{|\sigma,\sigma,\sigma,-\sigma\rangle, |\sigma,\sigma,-\sigma,\sigma\rangle, |\sigma,-\sigma,\sigma,\sigma\rangle, |-\sigma,\sigma,\sigma,\sigma\rangle\}.$$

The matrix is

$$\begin{pmatrix}
-\frac{J(2\alpha+1)}{4} & \frac{J}{4} & \frac{\alpha J}{2} & 0 \\
\frac{J}{4} & -\frac{J(2\alpha+3)}{4} & \frac{J}{2} & \frac{\alpha J}{2} \\
\frac{\alpha J}{2} & \frac{J}{2} & -\frac{J(2\alpha+3)}{4} & \frac{J}{4} \\
0 & \frac{\alpha J}{2} & \frac{J}{4} & -\frac{J(2\alpha+1)}{4}
\end{pmatrix}$$

- $n = 4$ $S^z = 0$

I used the basis

$$\{|\sigma,\sigma,-\sigma,-\sigma\rangle, |\sigma,-\sigma,\sigma,-\sigma\rangle, |\sigma,-\sigma,-\sigma,\sigma\rangle,$$
$$|-\sigma,\sigma,\sigma,-\sigma\rangle, |-\sigma,\sigma,-\sigma,\sigma\rangle, |-\sigma,-\sigma,\sigma,\sigma\rangle\}.$$

The matrix is

$$\begin{pmatrix} -\frac{J(2\alpha+1)}{2} & \frac{J}{2} & \frac{\alpha J}{2} & \frac{\alpha J}{2} & 0 & 0 \\ \frac{J}{2} & -J & \frac{J}{4} & \frac{J}{4} & 0 & 0 \\ \frac{\alpha J}{2} & \frac{J}{4} & -\frac{J(2\alpha+1)}{2} & 0 & \frac{J}{4} & \frac{\alpha J}{2} \\ \frac{\alpha J}{2} & \frac{J}{4} & 0 & -\frac{J(2\alpha+1)}{2} & \frac{J}{4} & \frac{\alpha J}{2} \\ 0 & 0 & \frac{J}{4} & \frac{J}{4} & -J & \frac{J}{2} \\ 0 & 0 & \frac{\alpha J}{2} & \frac{\alpha J}{2} & \frac{J}{2} & -\frac{J(2\alpha+1)}{2} \end{pmatrix}$$

The matrices for U_2 and H_2U_2 are the same as for U_1 and H_1U_1. The matrix elements for two spins are easily calculated from the singlet and triplet matrix elements.

References

[1] J. G. Bednorz and K. A. Müller, Z. Phys. B64, (1986) 189.

[2] F. C. Zhang and T. M. Rice, Phys. Rev. B37 (1988) 3759.

[3] P. W. Anderson, Science 235 (1987) 1196.

[4] E. H. Lieb and F. Y. Wu, Phys. Rev. Lett. 20 (1968) 1445.

[5] C. N. Yang, Phys. Rev. Lett. 19 (1967) 1312.

[6] J. E. Hirsch, Phys. Rev. Lett. 20 (1968) 1445.

[7] P. A. Bares and G. Blatter, Phys. Rev. Lett. 64 (1990) 2567.

[8] F. F. Assaad and D. Würtz, Phys. Rev. B. (1991) in print, IPS Research Report No. 90-18.

[9] M. Ogata, M. U. Luchini, S. Sorella and F. F. Assaad, Phys. Rev. Lett. 66 (1991) 2388.

[10] N. Metropolis, A. R. Rosenbluth, M. N. Rosenbluth, A. H. Teller and E. Teller, J. of Chem. Phys. 21 (1953) 1087.

[11] M. Suzuki, Prog. of Theor. Phys. 56 (1976) 1454.

[12] H.F. Trotter, Proc. Am. Math. Soc. 10 (1959) 545.

[13] M. Suzuki (editor), Quantum Monte Carlo Methods, Springer Series in Solid-State Sciences 74, Springer Verlag Berlin Heidelberg New York London Paris Tokyo (1987).

[14] N. Furukawa and M. Imada, Technical Report of ISSP A, No. 2326 (1990); to appear in J. Phys. Soc. Jpn.

[15] C. K. Majumdar and D. K. Ghosh, J. of Math. Phys. 10 (1969) 1388 and 1399.

[16] M. Ogata and H. Shiba, Phys. Rev. B41 (1990) 2326.

[17] M. Ogata, to be published.